

FREEZE FOAMING: A NOVEL PROCESS FOR THE SYNTHESIS OF
FOAM CERAMICS

by

Nathaniel Peyton Johnson

A thesis submitted in partial fulfillment
of the requirements for the degree

of

Master of Science

in

Mechanical Engineering

MONTANA STATE UNIVERSITY
Bozeman, Montana

April 2018

©COPYRIGHT

by

Nathaniel Peyton Johnson

2018

All Rights Reserved

ACKNOWLEDGEMENTS

Without the help of my professors and lab mates this thesis would never have happened. Dr. Sofie has been a tremendous help and this thesis would never have been completed without the help and guidance that you have given me. I would like to thank you for giving me an opportunity to work in lab and everything that you have done for me. I would like to thank my committee members Dr. Gannon and Dr. Ryan for reviewing my thesis and giving back helpful feedback. Also, I would like to thank everyone in the lab that has helped me out and answered all of the questions that I have including Dr. David Driscoll, Dr. Clay Hunt, Julie Muretta, Marley Zachariasen, Stephen Heywood, and John Kent. My family and friends deserve a special thanks for helping me throughout my academic career especially my mother Bonnie Barnhart, my girlfriend Jackie Bastine, my sister Megan Miranda, and my uncle Bruce Barnhart. Lastly, I would like to thank anyone who has helped me along the path to success.

TABLE OF CONTENTS

1. INTRODUCTION	1
2. BACKGROUND	3
Ceramics	3
Ceramic Bonds	6
Mechanical and Thermal Properties of Ceramics	10
Physics of Bubbles	12
Sintering	14
Ceramic Foams	18
Manufacturing Techniques	19
Direct Foaming	21
Replica Templating	24
Sacrificial Templating	26
Novel Techniques	27
Constitutive Properties of Foams	28
3. RESEARCH OBJECTIVE	32
4. EXPERIMENTAL PROCEDURE	34
Materials	34
Freeze Foaming	35
Slurry Preparation	35
Ball Milling	36
Bubble Formation and Simultaneous Freezing	36
Sintering	38
Parameter Identification	39
Solids Loading	39
Binder Concentration	40
Foam Volume Expansion Ratio	41
Pressure	42
Density Measurement	43
Microstructure	43
Compression Testing	44
5. RESULTS & DISCUSSION	47
Casting Parameters	47
Physical and Structural Properties	54
Mechanical Properties	62

TABLE OF CONTENTS CONTINUED

Sintering Characteristics	73
Demonstration of Freeze Foaming with Other Materials	75
Yttria Stabilized Zirconia.....	75
Metals.....	77
6. CONCLUSIONS.....	80
Future Work	81
REFERENCES CITED.....	82

LIST OF TABLES

Table	Page
1. Material Properties	11
2. Aluminum Oxide Properties	12
3. Solid Loading Study Samples	40
4. Binder Concentration Study Samples	41
5. Foam Volume Expansion Ratio Study Samples	42
6. Comparison of Foaming Techniques	61

LIST OF FIGURES

Figure	Page
1. Tiny “Snowman”	2
2. Uses of Ceramics	4
3. Types of Ceramics	5
4. Covalent Bond	7
5. Ionic Bond.....	8
6. Directionality of Ionic Bonds.....	10
7. Densification of alumina.....	15
8. Sintering Mechanisms.....	16
9. Structure of Ceramic Foam.....	16
10. Pyrolysis Treatment.....	17
11. Types of Foam Cells.....	19
12. Foam Extruder	20
13. Direct Foaming.....	21
14. Surfactant Stabilization	23
15. Particle Stabilization.....	24
16. Replica Templating	25
17. Sacrificial Templating	27
18. Repeatable Cellular Structure.....	29
19. Brittle Crushing	31
20. Research Objective Tree	33

LIST OF FIGURES CONTINUED

Figure	Page
21. Ball Milling	36
22. Vacuum Freeze Dryer System.....	37
23. Thermal Treatment	39
24. Light Microscope System.....	44
25. Compression Testing System	45
26. Compression Testing Sample Holder.....	46
27. Solids Loading Study Results.....	48
28. Binder Concentration Study Results (5% and 20% SL).....	49
29. Binder Concentration Study Results (30% SL).....	50
30. Foam Volume Expansion Ratio Study Results	51
31. Bubble Formation and Freezing	52
32. Cross Section of Ceramic Samples	54
33. Porosity vs. Binder Concentration.....	56
34. Pore Size vs. Binder Concentration.....	57
35. Porosity vs. Solids Loading.....	58
36. Pore Size vs. Solids Loading	59
37. Porosity vs. Foam Volume Expansion Ratio.....	59
38. Pore Size vs. Foam Volume Expansion Ratio.....	60
39. Difference in Porosity Measurements	61
40. Compression Testing Results	62

LIST OF FIGURES CONTINUED

Figure	Page
41. Progressive Failure in Ceramic Foam	63
42. Different Sections of Compression Testing	64
43. Acoustic Emissions during Compression Testing.....	65
44. Modulus vs Relative Density	66
45. Modulus vs Relative Density with Estimated Curve.....	67
46. Modulus vs Relative Density with Adjusted Curve	68
47. Compressive Strength vs Relative Density with Adjusted Curve	65
48. Comparison of Foam Structure	70
49. Relative Young's Modulus vs Relative Density	71
50. Relative Compressive Strength vs Relative Density	73
51. Microstructure of Various Foams.....	75
52. YSZ Foam	76
53. Aluminum Foam.....	78
54. Copper Foam	79

NOMENCLATURE

To keep track of different types of foams a short hand was developed. The naming scheme follows the structure, XX/XX – XX. The first number is the solids loading of the foam by volume. The second number is the binder concentration, which is the ratio of the weight of binder and powder. The third number is the foam volume expansion ratio, which is the ratio of the original slurry volume to the volume of the expanded foam. For example a foam sample by the name of 30/0.7 – 10 has a solids loading of 30%, a binder concentration of 0.7, and a foam volume expansion ratio of 10.

ABSTRACT

Foam is a class of materials that was developed only after World War II and ceramic foams are still in development. Many of the processes for synthesizing ceramic foam require the burning out of a polymer scaffold or the use of chemical reactions to generate pores. This thesis investigates the development of a novel synthesis approach called freeze foaming. In the freeze foaming process, pores are made by putting an aqueous solution under vacuum. The reduced pressure causes the air within the slurry to expand and form bubbles. Then once the foam is formed, it is frozen into place. Then the water is removed from the system through sublimation. Finally, the foam is densified by traditional sintering. After successfully creating ceramic foam samples, the parameters in the freeze foaming process were identified and investigated. Foam samples were characterized by taking density measurements, examining the macrostructure and microstructure with light microscopy, and determining mechanical properties through compression testing. In the end, highly porous foam samples with adjustable properties were synthesized using a novel manufacturing process.

INTRODUCTION

Ceramic foam is a unique class of materials that possess unique characteristics that have seen limited development due to limitations in manufacturing ceramics. Ceramic foams are perhaps most notable as lightweight thermal insulators that can be used in high temperature environments. There are three common synthesis techniques that are used to create ceramic foams including: direct foaming, replica templating, and sacrificial templating. Direct foaming incorporates pores by injecting air into a ceramic slurry. Replica templating is a process where a ceramic slurry is soaked up into a sponge to create a porous material, while polymeric beads are used in sacrificial templating to create ceramic foam.

Investigations into freeze-tape casting of ceramic materials for fuel cell application provided the impetus to study the fabrication of foams. The freeze casting process creates aligned pores in ceramic materials by freezing the liquid of a ceramic loaded slurry and removing it through sublimation. It was observed during freeze casting experimentation that slurry bubble droplets that hit the freezing bed produced a “snowman” structure, and hence the idea of freeze foaming was developed. During the down time of freeze tape casting, little “snowmen” were made by placing a bubble of aluminum oxide slurry onto a freezing aluminum bed in which, Figure 1 shows one “snowmen” that was made using the freeze tape caster. Compounding this serendipitous finding, during the traditional de-airing of a ceramic slurry, for freeze tape casting, the slurry and existing bubble content froze during the de-airing process from having the vacuum freeze dryer set at too low of a temperature. The subsequent foam structures that



Figure 1. The formation of a “snowman” structure made of aluminum oxide slurry was produced by placing bubbles of an aqueous slurry on top of each other and allowing them to freeze.

were observed in the ceramic materials gave rise to the concept of freeze foaming as a novel technique to form ceramic foam.

The focus of this thesis is to investigate a novel process to make ceramic foam. Within that research there were two different aspects. First, to develop the freeze foaming process and to determine the parameters that affect the foam synthesis. Second, to characterize the foam and to determine the effects of the processing parameters.

BACKGROUND

Ceramics

Ceramics are a class of materials that have a deep history and were first developed from natural materials, such as clay and other alumino-silicates. Humans have been using ceramics for thousands of years for a variety of utensils as well as artwork. It has been found that ceramics were used prior to 5000 BC (1). Ceramics are most famous for their use as toilets, bathroom sinks, and pottery however due to advancements in technology ceramics are used throughout industry in technical applications that require extreme hardness and temperature stability (1). Due to their unique material properties related to bonding, ceramics are used in numerous applications, in which Figure 2 shows some of the uses of ceramics. Ceramic materials are used in environments of extreme heat and some components of jet engines are made from ceramic materials, such as super-alloy blade coatings (10). Thermal insulation is perhaps the most notable usage aspect of ceramic materials in which the NASA space shuttles demonstrate their resilience in which the bottom surface of the space shuttle was lined with highly porous ceramic tiles to withstand the immense heat felt during the re-entry process. In addition to thermal insulation, ceramics are often used as electrical insulators. On high voltage electrical transmission lines, which are not coated with an insulating plastic, ceramics are used to keep electrical losses down therefore improving efficiency. Ceramic insulators are placed on overhead power lines where the electrical lines are supported and prevent electricity from flowing into the transmission towers. In more technical applications, ceramic



Figure 2. Examples of ceramic uses. Ceramic artwork from Montana artist Frances Sneska is shown in the upper left image (2). In the upper right image the silica fiber tiles on the space shuttle can be seen, black underside (4). The lower left image shows an electrical insulator used for transmission line, typically porcelain (5). Zirconia dental implants are depicted in the lower right image (3).

materials are used where other materials would simply not survive due to operational conditions of wear including dental implants, resistant coatings for various parts including cutting tools, and even ceramic coated as well as full ceramic ball bearings (1-8,10). Additionally, many common construction materials are a form of ceramic including; tile, cement/concrete, and brick. Ceramic materials have been a part of human society for a long time and they are used throughout industry in numerous applications with growing technical applications.

There are two different branches of ceramics which include traditional ceramics and advanced ceramics Traditional ceramics are composed of clay minerals such as porcelain, but include material likes cement and glass (8). Although traditional ceramics are important, this thesis will focus on advanced ceramics used in wear and insulation

application, however can be extended to functional ceramics used in electronic and energy applications. Advanced ceramics are split into oxides, such as aluminum oxide (Al_2O_3) which is a very common ceramic that is used for insulation, nitrides such as silicon nitride (Si_3N_4) which is used in engine parts, and carbides, such as boron carbide (B_4C) which is used for lightweight armor (7-8). The tree of ceramics can be seen in Figure 3. All ceramics consist of a metal atom bonding to a non-metal atom, except for allotropes of carbon, diamond graphite, graphene, and buckminsterfullerene aka buckyball.

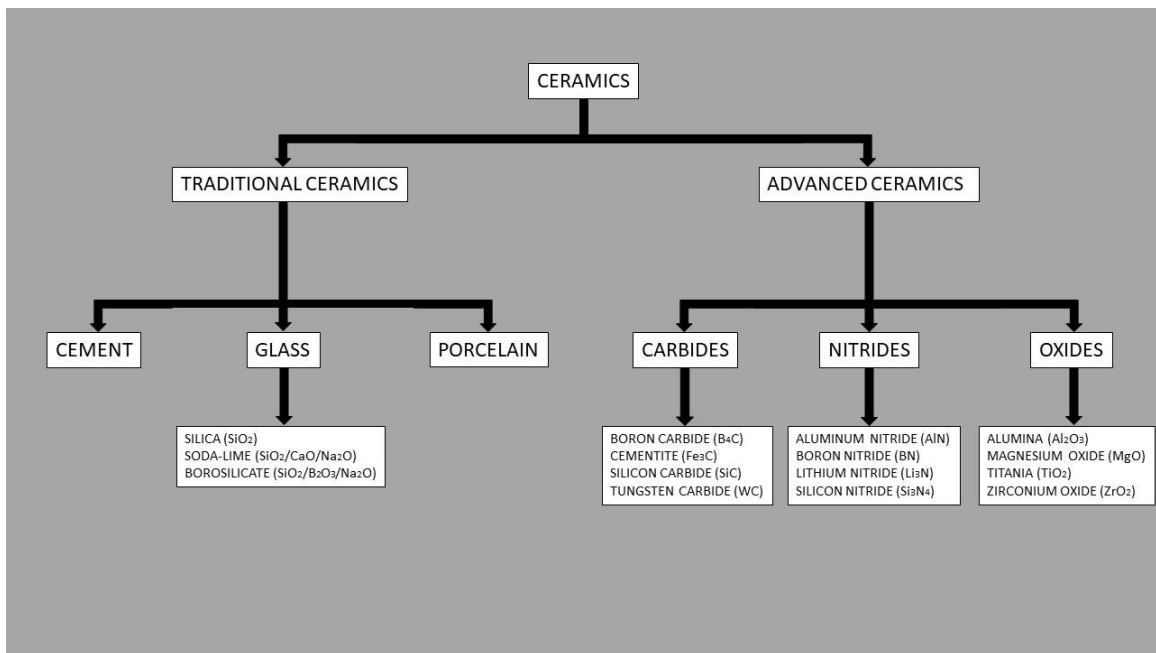


Figure 3. The different types of ceramics with the traditional ceramics depicted on the left side and advanced ceramics on the right side are shown. Examples of each type of ceramic are shown lower on the tree. Cement and porcelain do not have examples listed because they have a complex composition that contains many compounds. Of particular interest is the processing of oxide based ceramics that yield simplified sintering in atmospheric conditions to consolidation particulate into solid forms.

Ceramic Bonds

Ceramic materials are characterized by their covalent and ionic bonding which yields a departure from ductile metallic behavior due to inability to displace atoms/ions without breaking bonds. Ceramics are typically described as covalently bonded or ionically bonded, however it is more likely a mixture of covalent and ionic bonds. Covalent bonds are formed when electrons are “shared” by ions. In reality covalent bonds are formed when two ions have orbital overlap, this is the foundation of valence bond theory in which the electron wave functions of adjacent atoms interact to create a new wave function that facilitates coulombic cohesion. This orbital overlap attracts two ions to each other. There are two different components to covalent bonding, Sigma (σ) bonding and Pi (π) bonding. Sigma bonding is orbital overlap where electrons get shared, while pi bonding is where orbital alignment takes place, a form of van der Waals interaction. Sigma bonds are stronger than pi bonds due to the fact that actual overlap is occurring forming the classic covalent interaction. Covalent materials can be single, double, or triple bonded, however, the terminology does adequately describe the bonding nature of the material. When a covalent material has a single bond it is based upon the formation of a sigma bond. However, double bonded materials usually contain a sigma bond and a pi bond, as depicted in Figure 4. Furthermore, triple bonded covalent materials have one sigma bond and two pi bonds. Ethylene (C_2H_4) is a great example of a double bonded covalent material that contains both a sigma and pi bond. In this example the sp^2 bonded carbon has a double covalent bond. Between the two adjacent carbon

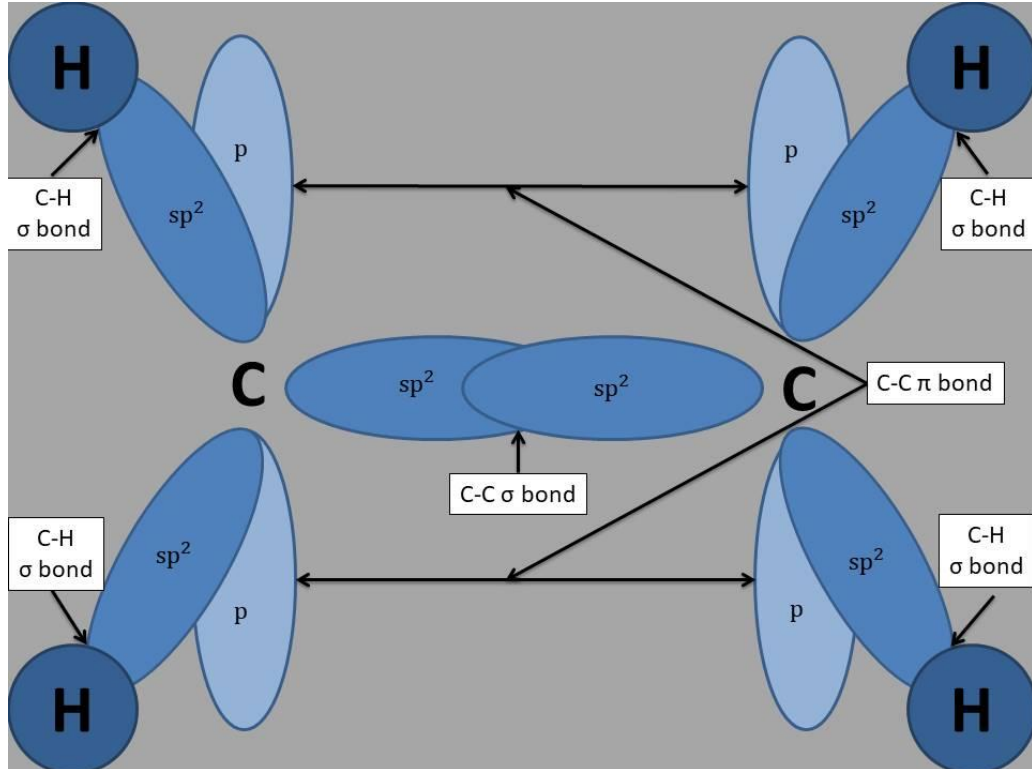


Figure 4. The covalent bonds of Ethylene are highlighted. The bonds of interest are the carbon-carbon bonds. In this material the carbons are double bonded together with one sp^2 orbital overlapping causing a sigma bond and the p orbitals of the carbon are aligned.

atoms there is orbital overlap or a sigma bond. While the other two orbitals of the carbon atoms extend to bond to hydrogen, one orbital of the carbon extends up and down. The carbon orbitals are aligned forming a pi bond. It should be noted that the hydrogen and carbon atoms form a sigma bond where orbitals and within the ethylene compound there is a total of six bonds, five sigma and one pi. The bonding configuration of ethylene can be seen in Figure 4 where the sigma and pi bonds are highlighted. Due to the orbital overlap, covalent bonds are short and stiff which is quite beneficial, but they are highly directional which limits ductility as atom are not able to be strained plastically without breaking the covalent orbital overlap of the sigma bond.

Ionic bonding in ceramic occurs when electrons are transferred between atoms to create cations, positively charged ions, and anions, negatively charged ions. This charge difference between ions forces the ions to attract to each other and forms a bond that has an overall neutral charge. One very common example of this bond is sodium chloride (NaCl) or more commonly known as table salt. In this material sodium, an anion, transfers an electron to chlorine, a cation. The transfer of an electron causes the two ions to attract to one another and the entire system has a neutral charge. Figure 5 shows the formation of an ionic bond in sodium chloride. Ionic bonds are not as short or stiff as

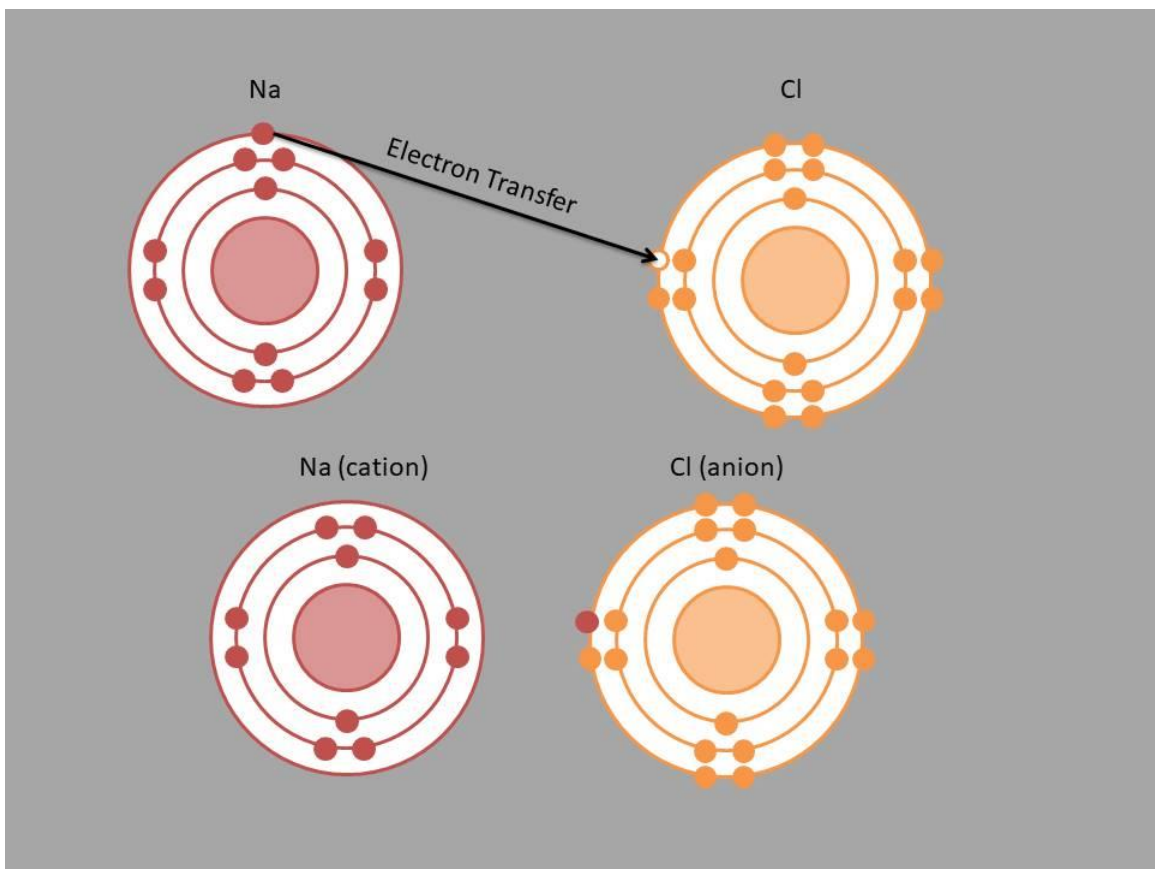


Figure 5. The formation of sodium chloride is depicted. An electron is transferred from sodium to chlorine to form a cation of sodium and an anion of chlorine. Overall a charge neutral sodium chloride compound is formed with an ionic bond.

covalent bonds but they are shorter and stiffer than metallic bonds as evidenced in the hardness of materials which correlates with strength. While ionic bonds are not direction sensitive, like covalent bonds, in a bulk material they are position sensitive yielding brittle behavior common across all ceramics. If ionically bonded materials are pushed into the wrong position, ions with like charges will be pushed into close proximity in which the bonds will break as the ions repulse each other due to equal charge values, a depiction of this position sensitivity can be seen in Figure 6. Materials can share electrons equally and transfer electrons, but generally most chemical compounds do not behave in this manner. Electron sharing varies from almost equal sharing, mainly covalent, to the electron being mostly held by one ion, mainly ionic (9, 11).

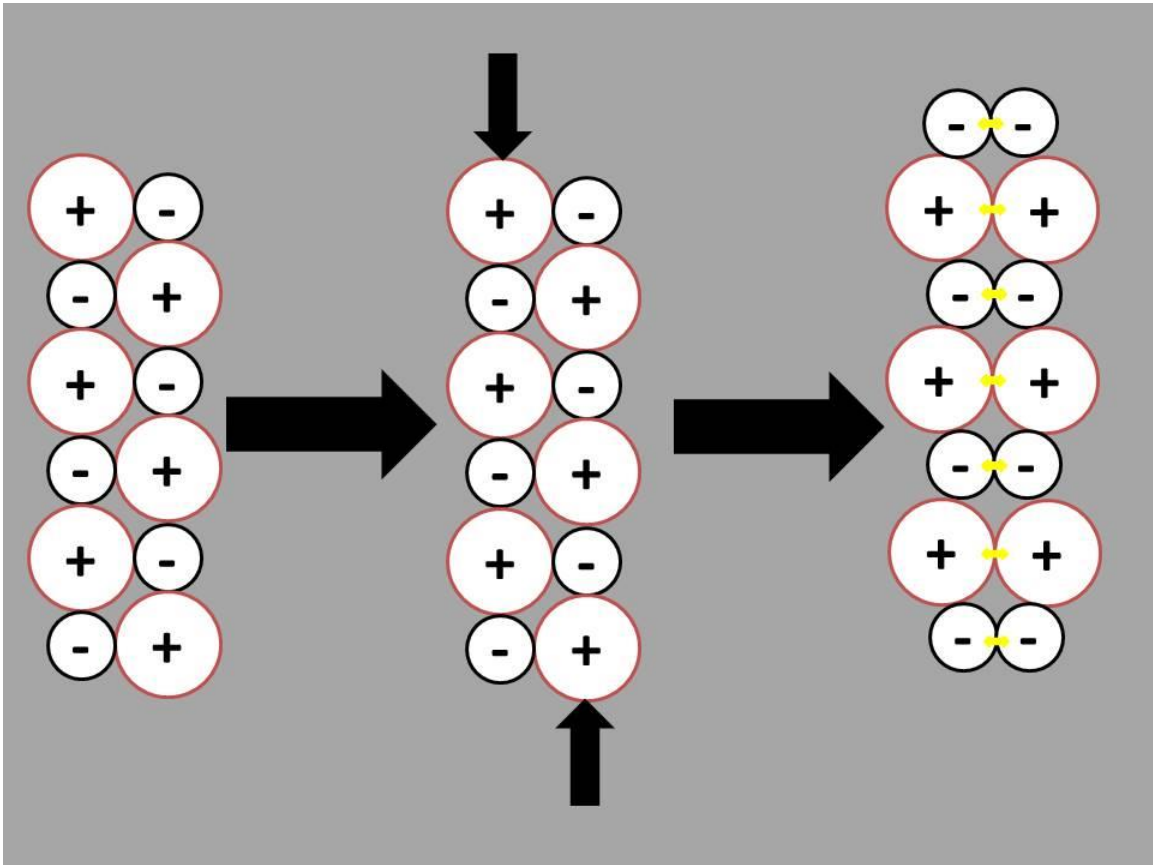


Figure 6. Depiction of direction sensitivity for ionic bonds is shown. Outside forces drive ions to shift into different positions, where repulsive forces are shown as yellow arrow and the ions push each other apart.

Mechanical and Thermal Properties of Ceramics

The unique material properties of ceramics; high melting temperature, low thermal expansion, high elastic modulus, low density, low thermal and electrical conductivity, and low fracture toughness are all derived from the bond type of ceramic materials. Looking at the first few properties listed; high melting temperature, low thermal expansion, and high elastic modulus, these properties can be explained due to the shorter, stiffer bonds associated with covalent and ionic character. The stiff bonds make it so that large amounts of energy are needed to move atoms apart from each other. Low

Table 1. The material properties of a few ceramics, metals, and polymers have been selected. The polymer melting temperatures provided are actually glass transition temperatures (7).

Material Properties of Various Materials						
Material	Melting Temperature (°C)	Coefficient of Thermal Expansion ($10^{-6}/^{\circ}\text{C}$)	Elastic Modulus (GPa)	Thermal Conductivity (W/(m·K))	Electrical Resistivity ($\mu\Omega\cdot\text{cm}$)	Fracture Toughness ($\text{MPa}\cdot\text{m}^{0.5}$)
Ceramics						
Aluminum Oxide	2004 - 2096	7 - 10.9	215 - 413	30 - 38.5	1^*10^{20} - 1^*10^{22}	3.3 - 4.8
Aluminum Nitride	2397 - 2507	4.9 - 6.2	302 - 348	80 - 200	1^*10^{19} - 1^*10^{21}	2.5 - 3.4
Boron Carbide	2372 - 2507	3.2 - 3.4	400 - 472	40 - 90	1^*10^5 - 1^*10^7	2.5 - 3.5
Silicon Nitride	2388 - 2496	3.2 - 3.6	280 - 310	22 - 30	1^*10^{20} - 1^*10^{21}	4.0 - 6.0
Metals						
Aluminum Alloys	475 - 677	21 - 24	68 - 82	76 - 235	2.5 - 5.0	22 - 35
Cast Irons	1130 - 1250	10 - 12.5	165 - 180	29 - 44	49 - 56	22 - 54
Copper Alloys	982 - 1082	16.9 - 18	112 - 148	160 - 390	1.7 - 24	30 - 90
Titanium Alloys	1477 - 1682	7.9 - 11	90 - 120	5.0 - 12.0	100 - 170	14 - 120
Polymers						
Epoxy	N/A	58 - 117	2.35 - 3.075	0.18 - 0.5	1^*10^{20} - 6^*10^{21}	0.4 - 2.22
Nylon	44 - 56*	144 - 150	2.62 - 3.2	0.23 - 0.25	1^*10^{19} - 1.5^*10^{20}	2.22 - 5.62
Polyethylene	-25 - -15*	126 - 198	0.621 - 0.896	0.40 - 0.44	3^*10^{22} - 3^*10^{24}	1.44 - 1.72
Teflon	107 - 123*	126 - 216	0.4 - 0.552	0.24 - 0.26	3^*10^{23} - 3^*10^{24}	1.32 - 1.8

thermal and electrical conductivity are explained by the fact that covalent and ionic bonds more or less lock the electrons of the atoms into well-defined and discrete electron energies. Electrons in this manner that lack a band structure are not allowed to freely travel through the material, because of this electrical conduction through the bulk of a ceramic material is limited. The bond directionality and position sensitivity of ceramic materials, whether by covalent or ionic bonding explains the brittle behavior of ceramics and hence the low fracture toughness. As atoms/ions are displaced well beyond their equilibrium bond radius, directionality yields failure of the bond or atoms will actually start to repulse each other due to equal charge values. Table 1 shows the material properties of certain ceramics, metals, and polymers for a comparison of ceramic materials to other materials. Often regarded as the steel of the ceramics industry, the main

Table 2. The material properties of aluminum oxides are provided. The range of material properties comes from different purities and sized alumina (7).

Material Properties of Aluminum Oxide		
Density	3.5 - 3.98	g/cc
Melting Temperature	2004 - 2096	°C
Coefficient of Thermal Expansion	7 - 10.9	$10^{-6}/^{\circ}\text{C}$
Thermal Conductivity	30 - 38.5	W/(m·K)
Electrical Resistivity	$1 \cdot 10^{20} - 1 \cdot 10^{22}$	$\mu\Omega \cdot \text{cm}$
Elastic Modulus	215 - 413	GPa
Compression Strength	690 - 5500	MPa
Tensile Strength	350 - 665	MPa
Fracture Toughness	3.3 - 4.8	$\text{MPa} \cdot \text{m}^{0.5}$

material used for this research was aluminum oxide, in which Table 2 provides more material properties for aluminum oxide.

Physics of Bubbles

The physics of bubbles is well understood (19,31), however modeling the evolution of bubbles in foam is very difficult due to the fact that the principal physics spans a large scale of time and space. There are two different regions in clusters of bubbles or foam. First, there is the lamellae or bubble wall. Second, there is the region where different bubbles touch or the plateau border. Liquid foams are not stable and there are always three different dynamical movements occurring. The first dynamical movement is drainage. Drainage is the act of fluid flowing downward. The rate of drainage, or thinning of bubble walls is related to the viscosity of the fluid, μ , the density

of the fluid, ρ , the gravity acting tangential to the bubble wall, g_s , and the surface tension, σ . Saye and Sethian (19) have developed a fourth order partial differential equation that implements these components and needs two boundary conditions to be solved. This relationship can be seen in Equation 1. In addition, disjoining pressures and van der Waals interactions can be implemented into the model, which is necessary when looking at longer time scales. The second dynamical movement is coarsening.

Coarsening follows the same principle as Ostwald's ripening where small bubbles converge together to form larger and larger bubbles over time. The last dynamical movement is collapse. Collapse is where the faces of exposed bubbles rupture. This is a direct result of drainage and outside forces acting on the face of a bubble. Drainage continues until the bubble walls are too thin and the bubble ruptures displacing any leftover liquid into the surrounding bubbles (19, 31). Drainage, coarsening, and collapse can be slowed by the addition of surfactants or by particle modification. These additives have been shown to even stabilize foams for days.

Equation 1

$$\eta_t + \frac{1}{3\mu} \nabla_s \cdot \left(\sigma \eta^3 \nabla_s \left((k_1^2 + k_2^2) \eta + \Delta_s \eta \right) + \rho g_s \eta^3 \right) = 0$$

Where: η is the half thickness of the bubble wall

∇_s is the surface gradient

$\nabla_s \cdot$ is the surface divergence

Δ_s is the Laplacian on the curved surface of the lamella

$k_1 + k_2$ are the principal curvatures of the Laplacian

Based off of the research on bubbles, while synthesizing foam the three dynamical movements will need to be mitigated. Additionally, knowing how drainage, coarsening, and collapse effects bubbles will improve understanding on what processing parameters will have an effect on the synthesis of foam, such as viscosity.

Sintering

Sintering is the act of molecules, ions, or atoms diffusing through a solid. This process is most notably used in ceramics processing as a method to consolidate a green ceramic material comprised of particulate into a dense and strong structure. This process is driven thermodynamically the reduction of surface free energy as particles neck and grow to achieve a consolidated structure by atom transport in the solid state. While driven thermodynamically, atoms typically need sufficient thermal energy to allow sufficiently fast rates such that sintering is often performed at $2/3$ - $3/4$ of the melting temperature. With ceramics, green bodies are typically fabricated by processing means to consolidate particles into structures with 45 – 65% theoretical density. The high sintering temperatures provide a mechanism for the porosity to be diminished and the ceramic to achieve greater than 99% density under sufficient processing conditions. In this manner, densification has been achieved and is accompanied by increased mechanical properties of the ceramic. There are however, multiple mechanisms by which sintering occurs, but only two mechanisms are noted to drive densification; volume diffusion and grain-boundary. Volume diffusion is defined as atoms moving from the bulk of a particle to a new necking surface which grows between two adjacent particles. Grain-boundary

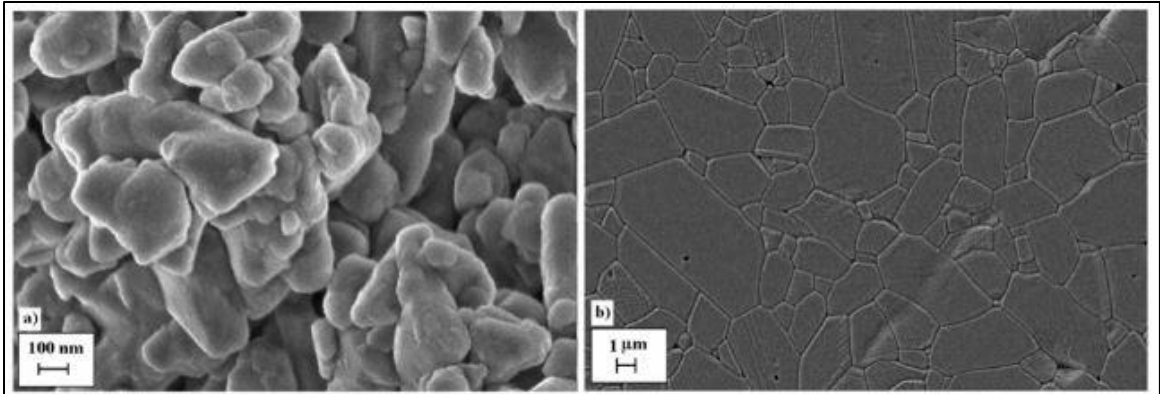


Figure 7. The densification of alumina through sintering are shown. Alumina was sintered at 1600 C (33).

diffusion is a different pathway where atoms move along the grain boundary of a particle and move to a necking surface. The effects of sintering on the structure of alumina can be seen in Figure 7 (33). Figure 8 shows these two sintering pathways where the first pathway is volume diffusion and the second pathway is particle diffusion. For sintering to take place one hump needs to be overcome to allow particle movement. The activation energy, or the thermal energy required for atom transport, must be met to achieve sintering (1,32).

Sintering of foams presents a different perspective with regard to densification. In preparing the ceramic foams, some porosity is intended to be retained, however, the regions that define the foam cell walls needs to density to facilitate rigidity of the structure. This relationship is illustrated in Figure 9. With insufficient cell wall integrity, the ceramic foam may not offer sufficient strength to support even thermal transport applications. Additionally, another key concern arises when sintering is performed on ceramic foams related to the manufacturing process. The sacrificial material (organic compound) that is used to form many ceramic foams requires pyrolysis. To perform

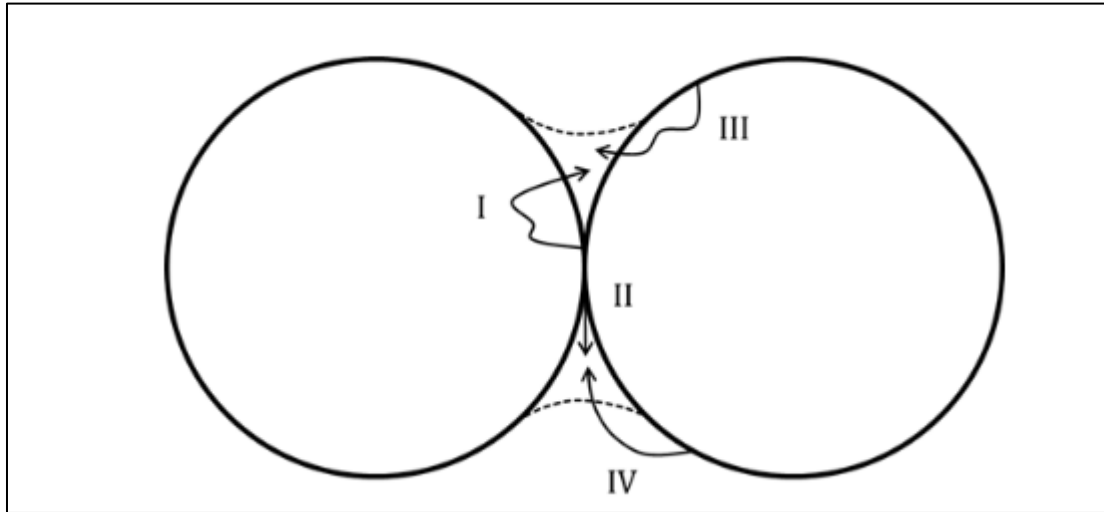


Figure 8. The two sintering mechanisms that contribute to densification are I, volume diffusion, and II, grain-boundary diffusion. Surface diffusion III and evaporation/condensation IV are noted to only coarsen the ceramic particles (32).

pyrolysis, the foam is heated to approximately 200°C and 600°C and held at that temperature to achieve sufficient burnout (24). During the pyrolysis step of sintering, the process cannot be performed too quickly as the structure can be damaged. If the material

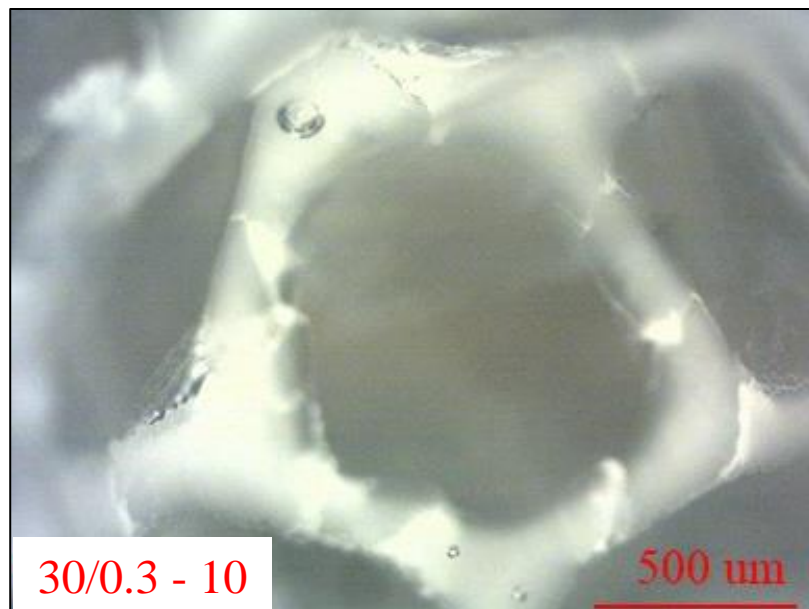


Figure 9. The structure of a ceramic foam has both rigid walls/struts and porosity.

is completely encapsulated in the strut of the foam, the internal pressures within the strut can build up too quickly and rupture the strut. In other situations, cracks can be introduced into the foam structure if the additives are volatilized too quickly. It has been observed that the burnout rate, for thin ceramic plates must be limited to 20 mg/min (34). Figure 10, shows a pyrolysis run needed to safely remove the organic template used in the synthesis of ceramic foam by sacrificial templating. This long time needed to achieve pyrolysis is a negative for the most traditional manufacturing techniques of ceramic foam.

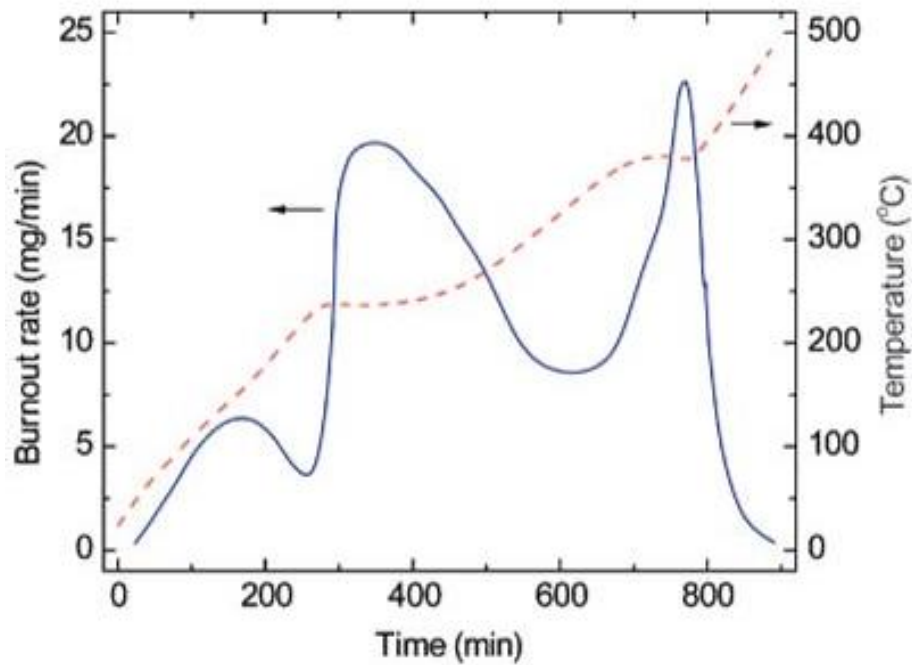


Figure 10. The two stage pyrolysis treatment of a sacrificial organic material, starch, used to synthesis alumina foam is depicted (34).

Ceramic Foams

There are several different kinds of foam whether comprised of polymer, metal or ceramic including closed cells, open cells, partially open cells, and mixed cells (23). The first type of foam, closed cell, is defined as foams that have material distributed on the struts of the bubbles as well as faces. This kind of foam has distinct cells that are encapsulated. Bubble wrap is a good representation of closed cell foam in which the bubbles entrain a fluid or gas. The second type, open cell foams, are a system of connecting struts that does not have material connecting between them. Due to the openness of the structure gasses and fluids can easily flow through this type of foam. The third type of foam, partially open cells, is similar to closed cell foam, but within the faces of the bubbles there are holes. The last type of foam, mixed cell, is a foam that contains both open and closed cell foam. Figure 11 shows the different types of foams.

Ceramic foams have numerous applications due to their low densities, high melting points, low thermal conductivity, and high corrosion resistance. Closed cell foams are great for thermal insulation. Ceramic foams with closed cells are used for high temperature insulation, including the insulation for furnaces. Open cell ceramics foams have been studied for the use as the scaffolds of batteries, electrodes, and solid oxide fuel cells (18,21,23,24). In addition, ceramic foams have been studied and used in applications including filtration of molten metals, the filtration of hot gases like exhausts gases, and even bone repair (18,24-26).

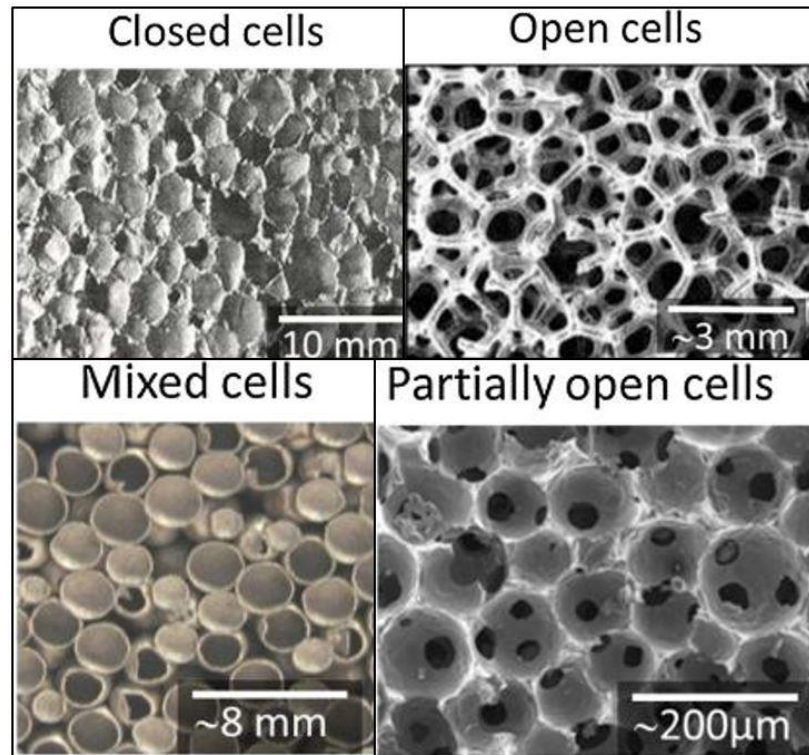


Figure 11. The different types of foams are shown. Each type of foam has different properties and is suitable for different types of applications (23).

Manufacturing Techniques

Foam from a general perspective is a relatively new class of engineered material, polymer foam was developed after World War II. By the 1960s mass production of polyurethane foam had begun, but humans have utilized for thousands of years (18). Wood, cork, and coral are all natural foams that humans have utilized for tools from building homes to keeping wine secure. Bones are even a foam structure found as a natural composite which has allowed them to be relatively light while retaining strength (10). Polymeric foams have been extensively developed and the most traditional manufacturing technique is foam extrusion. In foam extrusion a liquid polymer has gas incorporated into it. The gas, and porosity, are incorporated by stirring a bath causing

aeration, or by blowing a gas into it (ie. like a bubbler in an aquarium), but the most common method involves blowing agents. Blowing agents are chemicals that are mixed into the polymer system that create gas bubbles by decomposing while in the polymer (10,36). The most common types of blowing agents release either nitrogen, carbon monoxide, or carbon dioxide while decomposing (10,36). These agents are introduced into the molten polymer while it is in the barrel of the extruder or before entering the extruder. Some typical blowing agents are pentane (C_5H_{12}) and fluorocarbons (C_xF_y) such as trichlorofluoromethane ($CFCl_3$) and dichlorotetrafluoroethane ($C_2Cl_3F_4$) (36). Ceramic foams are not as developed as polymer foams, largely as a result of the high processing temperatures required with ceramics. As with polymers there are multiple processes used to create ceramic foam, but the three most developed techniques are direct foaming, replica templating, and sacrificial templating.

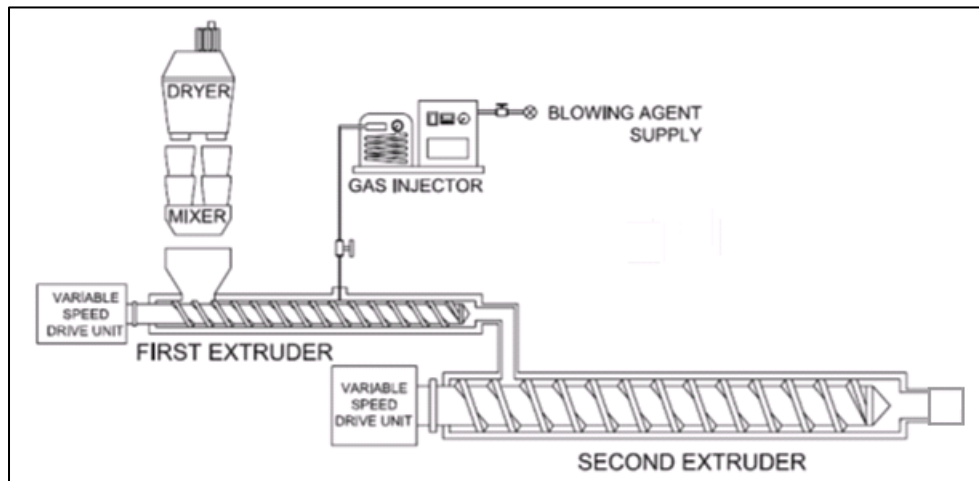


Figure 12. A two stage foam extruder is depicted where the blowing agent is incorporated through the barrel of the extruder (37).

Direct Foaming. Direct foaming is a process that is very similar to how polymeric foams are made. In this process gas is added to a slurry to form bubbles which becomes the pores in the foam. Gas can be introduced by mixing the slurry or by adding blowing agents. Blowing agents are just chemical compounds that when combined with another chemical release a gas. Two examples of blowing agents are sodium bicarbonate, more commonly known as baking soda, (28) and hydrogen peroxide (27). When baking soda decomposes carbon dioxide gas is released within the slurry which creates pores. Similarly when hydrogen peroxide decomposes oxygen gas is evolved. The gas introduced to the slurry forms bubbles which leads to pores within the foam. Once the bubbles are formed in the liquid slurry, the slurry has to be set so that the structure is permanent. Setting can be done by multiple types of additives or techniques. The most common method is using polymeric additives and inducing cross-linking (13,15-17,23,24,27). After the foam is set, it is dried and sintered. This leads to a pure ceramic foam. Figure 13, depicts the process of direct foaming (24).

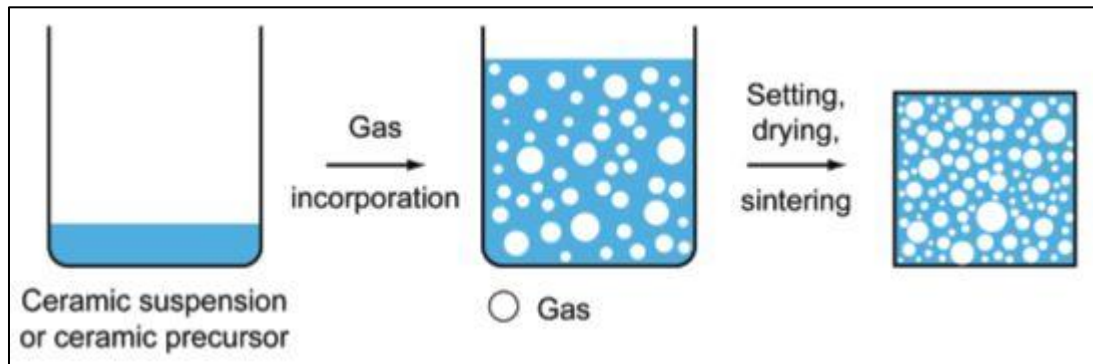


Figure 13. The basic steps of direct foaming are shown. (24)

The most challenging part of the direct foaming process is keeping the bubbles intact during setting. During the setting process coarsening and drainage must be

prevented or limited. To overcome Ostwald ripening, different additives are implemented into the ceramic foam slurry. There are two different stabilizing techniques that are used, surfactant stabilization and particle stabilization. Surfactants or, “SURFace ACTive AgeNT” have many definitions, but surfactants are any additives that help particles in a slurry act differently than they normally would. Surfactants can be used to alter surface energy, surface tension, surface charge, help disperse particles, or stabilize particles. Surfactants molecules are amphiphilic. They have two different regions, where one portion is polar and the other portion is non-polar. The slurry needs to be aqueous based in order for the surfactant to work. Surfactants stabilize foam by lowering the interfacial energy of the air and water boundary. The surfactant adsorbs to the surface and slows coalescence of bubbles in the foam. Using surfactants makes it so that different sized pores can be incorporated into the foam, ranging from 35 μm to 1.2 mm (24). Figure 14, shows how a surfactant interacts with the aqueous based foam while it is setting.

The other method to stabilize foams, via the direct foaming process, is using particles. Particles are altered so that they behave in the same way as the surfactants. The particles bunch at the interface between the air and water. This lessens the effects of Ostwald’s ripening and slows bubbles from combining. Figure 12, shows silica particles clustering at the air-water interface (35). The particles were altered using short chain amphipathic molecules. These molecules cause the particles to have a hydrophobic and hydrophilic side, thus causing bunching at the air-water interface within the foam. Particle stabilization is dependent on having a certain concentration of amphipathic molecules, but once the threshold is met the foam, becomes ultra-stable and it has been

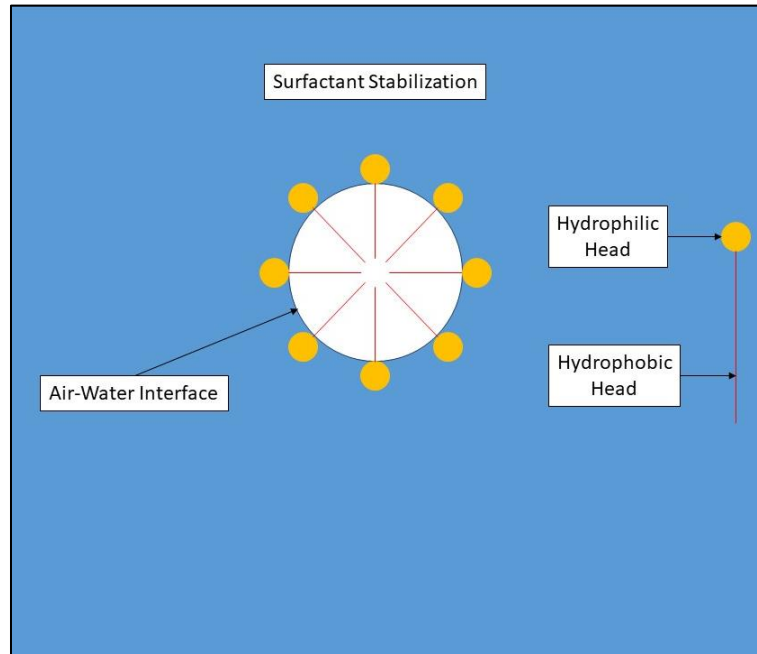


Figure 14. Surfactant stabilizing an air bubble in water is shown. Where the surfactant molecules form a "ring" which creates stable air bubbles.

shown that the coarsening of the bubbles can be deterred for as long as four days. This high stability makes it so that the foam does not need to be set by gelation and can be dried once the foam has been formed. Particle stabilized foam can have pores that range from 10 to 300 μm . In addition, foams made using this process have been able to achieve porosity levels of 93% (15,17,24).

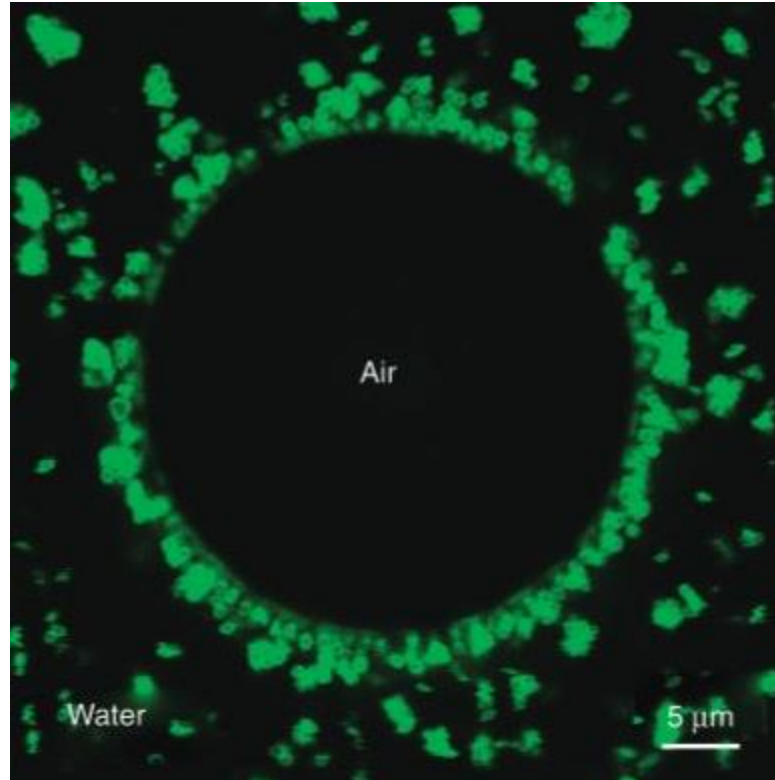


Figure 15. Silica particles are shown to lock together at the air-water interface through a confocal microscopy image. The silica particle surfaces were made hydrophobic using hexyl amine (35).

Replica Templating. Replica templating is a manufacturing technique for ceramic foams. This process can be seen in Figure 16. Replica Templating is the oldest manufacturing technique used to make macroporous ceramic foams, dating back to the 1960s. At first, the technique was done using polymeric sponges with high porosity (24). Today, replica templating is the most used manufacturing technique for ceramic foams where the templates are generally made of open cell polyurethane. Replica templating is a simple technique that can be used with almost any material system with little modification. These reasons are why the technique is so heavily used in industry, but the fact that the template must be removed increases the time required to synthesis parts and

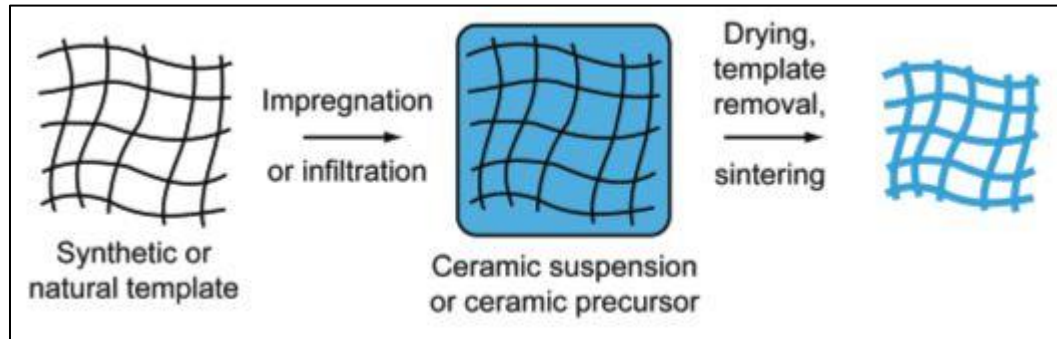


Figure 16. The steps of replica templating are shown (24).

a lot of sacrificial material is used that needs to be burned out of the foam and releases gases like carbon dioxide (23,24).

In the replica templating technique, a polymeric sponge is placed into a suspension of ceramic particles until the sponge is fully saturated. Then, excess material is removed from the sponge by squishing the sponge using rollers. Once the correct amount of suspension is in the template, the foam is dried and the template is removed through pyrolysis. During this step the foam is heated very slowly until the template is completely removed and only the ceramic particles remain. Heating is done at rates less than $1^{\circ}\text{C}/\text{min}$. Pyrolysis occurs by heating the ceramic infused template up to 800°C (24). The template must slowly be removed so that during pyrolysis the struts in the foam structure do not collapse due to too quick of polymer migration or too high of pressure build up within the struts. Lastly, the ceramic particles are fully densified by sintering the foam at the appropriate temperature. As mentioned previously the template is generally made of polyurethane, but this process has also been shown to work with natural templates like coral and wood. Using this process foams can be made with pore sizes varying from $200\mu\text{m}$ to 3mm . The foam is limited to pores larger than $200\mu\text{m}$ due to the

fact that it is difficult to create polymeric templates with openings smaller than 200 μm . Porosity levels ranging from 40% to 95% have been achieved using replica templating (16,23,24).

Sacrificial Templating. Sacrificial templating is a process where ceramic particles and some type of sacrificial material are combined into a homogeneous mixture. Then the sacrificial material is removed allowing the ceramic particles to be sintered. The material that is extracted from the foam leaves behind pores. Figure 17, shows the sacrificial templating method. This process is robust and has been shown to work with many different material systems.

There are a variety of materials used as the sacrificial material including polymers, salt, metals, and liquids including water (14,16,23,24). The sacrificial templating manufacturing technique differs substantially based on the type of sacrificial material chosen. These sacrificial materials are combined with the ceramic particles by various means. The ceramic particles and sacrificial material can be combined into a suspension where the mixture is then casted. Or, more commonly dry powder forms of the ceramic and sacrificial material are combined and pressed into a mold. Then, depending on the type of sacrificial material used the material is removed by various means. For sacrificial material such as polymers, the material is removed by thermal treatment. The foam is heated up to 600 $^{\circ}\text{C}$ where pyrolysis takes place (24). The sample must be held at this temperature for a long time and slow heating rates must be used to not damage the foam structure. Another removal process is the use chemicals. This process is done for sacrificial material such as salts and metals. In the case of salt,

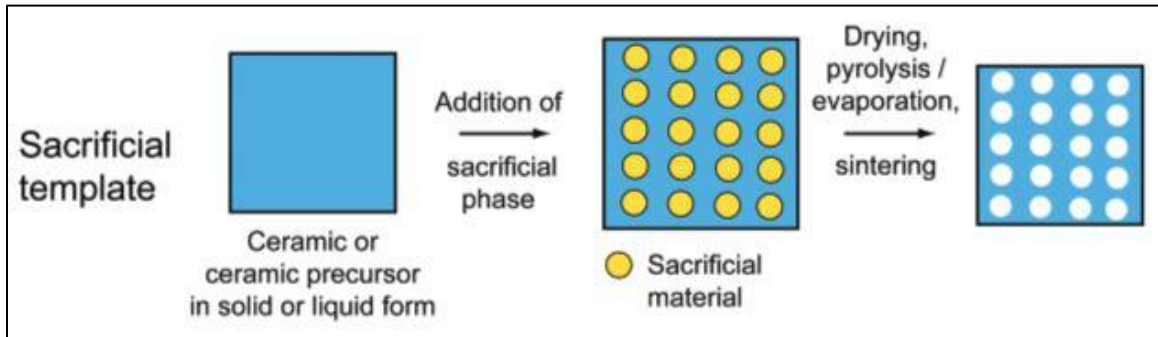


Figure 17. The steps of sacrificial templating are shown (24).

multiple washings using water has been shown to remove the salt, while metals generally need to be removed using acid. Lastly, sacrificial material like water or other liquids can be removed through evaporation or sublimation. After the sacrificial material has been removed, the ceramic foam is strengthened through traditional sintering methods. Using sacrificial materials, porosity levels ranging from 20% to 90% can be achieved with pore sizes ranging from 1-700um (16,23,24).

Novel Techniques. There are multiple groups researching novel foam synthesis techniques (43,45). Jayasinghe and Edirisinghe developed a technique where polyurethane foam was electrospayed with a slurry of alumina. With this technique they obtained an open cell foam with a porosity of roughly 96% that replicated the polyurethane template with extreme accuracy (43). Li, et. al., synthesized silver sulfide (Ag_2S) porous foam by placing a suspension of silver sulfide and hexane on top of diethylene glycol. When the system was exposed to air the hexane evaporated and left behind a porous structure of silver sulfide (45). Other groups are researching synthesis techniques that are not foams but results in similar porous structures (14,44). Nishihara, et. al., created a honeycomb structure of silica using ice templating, where a hydrogel was

utilized to form a silica framework and then the structure was frozen by dipping the structure into a cold bath set to -30°C (14). Hong, et. al., created interconnected pore channels in a zirconia structure by utilizing camphene slurries of zirconia and freezing them at 5°C . This technique successfully created samples that had porosities ranging from 67% to 82% (44).

Constitutive Properties of Foams

Ceramic foams have many of the same properties that are seen in fully densified ceramics such as high melting temperature, low electrical and thermal conductivity, and low thermal expansion. The properties of foam are heavily tied to how much gas is incorporated into the foam, Ashby and Mehl (38) were the first to show the relationship between the relative density and mechanical properties of cellular solids in 1983. Equation 2 shows the relationship of relative density, R_{ρ} , where ρ is the density of

Equation 2

$$R_{\rho} = \frac{\rho}{\rho_s}$$

the foam and ρ_s is the density of a fully densified solid of the same material. The relationship of relative density can also be determined by examining the structure of the foam. Equations 3 and 4 show the relationship between the thickness of the struts of the foam, t , and the length of the struts, l . Figure 18 shows where the strut thickness and length can be found on a foam sample. Equation 3 is valid for foams that are open cell,

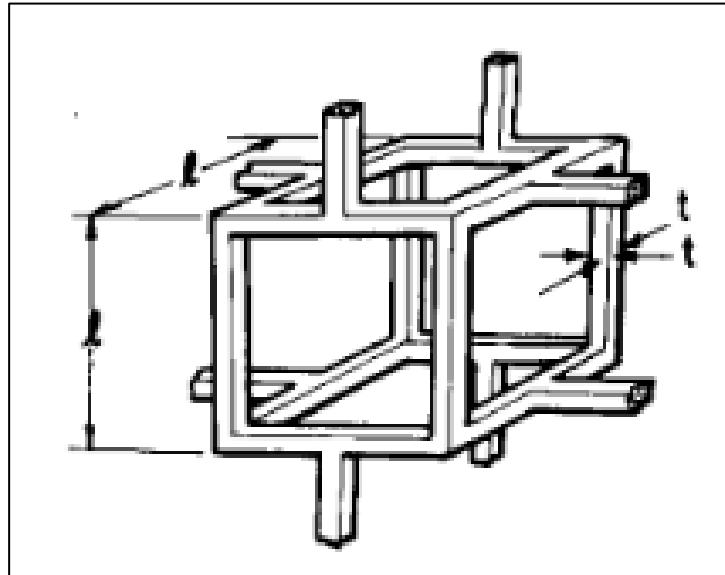


Figure 18. The cellular unit used in the Ashby and Mehl model, where the thickness and length used for relative density are shown (38).

Equation 3

$$\frac{\rho}{\rho_s} = \left(\frac{t}{l}\right)^2 \quad (\text{Valid for Open Cell Foams})$$

Equation 4

$$\frac{\rho}{\rho_s} = \left(\frac{t}{l}\right) \quad (\text{Valid for Closed Cell Foams})$$

while Equation 4 is valid for foams with closed cells. Then, to relate the relative density to porosity Equation 4 is used, where P is porosity. It was found that for a cellular solid

Equation 5

$$P = 1 - R_\rho$$

that the ratio of elastic modulus is proportional to the squared value of relative density for open cell structures and by the cubed value of relative density for closed cell structures.

Equations 6 and 7 show the relationships of elastic modulus, where E_S is the elastic

Equation 6

$$E = E_S \left(\frac{\rho}{\rho_S} \right)^2 \quad (\text{Valid for Open Cell Foams})$$

Equation 7

$$E = E_S \left(\frac{\rho}{\rho_S} \right)^3 \quad (\text{Valid for Closed Cell Foams})$$

modulus of the solid material. Also it should be noted that the E_S term has been moved from the left side of the equation to the right side as presented. Ashby and Mehl also looked at how brittle materials like ceramics and certain plastics fail. They determined a relationship for brittle crushing, which is the mechanism by which ceramic foams fail due to compressive forces. Figure 19, shows the brittle crushing mechanism where cracks propagate through certain struts of the foam, while other struts stay intact. They determined that the relative density relates to the ratio of crushing strength by a factor of 3/2 for open cells and a factor of two for closed cells with a factor of 0.65. Equations 8 and 9 show the relationship for the crushing strength where σ_f^* is the crushing or compressive strength of the foam and σ_f is the compressive strength of the fully densified solid. Again, σ_f has been moved to the right side of the equation.

Equation 8

$$\sigma_f^* = 0.65\sigma_f \left(\frac{\rho}{\rho_s}\right)^{3/2} \quad (\text{Valid for Open Cell Foams})$$

Equation 9

$$\sigma_f^* = 0.65\sigma_f \left(\frac{\rho}{\rho_s}\right)^2 \quad (\text{Valid for Closed Cell Foams})$$

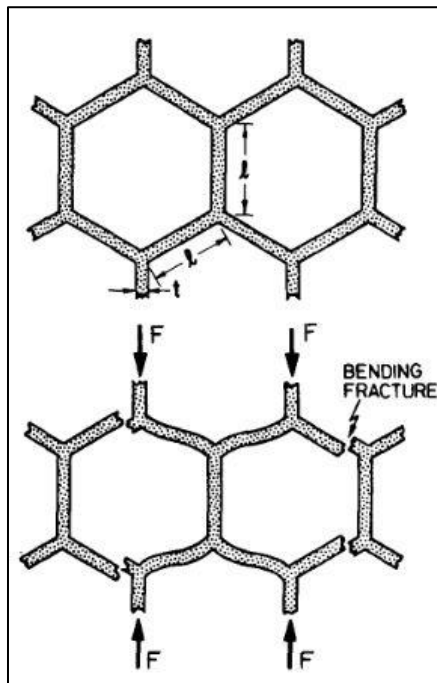


Figure 19. The mechanism of failure for brittle solid cellular structures, brittle crushing (38).

RESEARCH OBJECTIVE

The objective of this thesis is to develop a novel approach to making ceramic foam through a route of freezing and sublimation. Within that objective there are three discrete goals that need to be met so that the overall objective is accomplished. First, ceramic foam needs to be successfully synthesized and sintered into a solid structure that retains sufficient strength for physical and mechanical properties characterization. To meet this goal the process of freeze foaming needs to be developed including the detail of the processing parameters and organic additives. Then it needs to be demonstrated that ceramic foam can be synthesized using the freeze foaming process.

Second, the foam needs to be characterized and tested to determine the properties and how those properties scale with the currently accepted behavior of cellular materials. Once the parameters of the freeze foaming process have been established, multiple samples with the same properties can be made for characterization in which the properties of the foam can be ascertained. To reach this goal, three different properties will be investigated; physical properties, structural properties, and mechanical properties. The physical properties examined will be the density of the foam and the relative density of the foam. Next, to investigate the structural properties the pore size and porosity will be evaluated. Finally, the mechanical properties will be investigated by calculating the theoretical elastic modulus and compressive strength which will be contrasted with the empirical elastic modulus and compressive strength.

Third, all of the parameters within the freeze foaming process needs to be identified and examined. Once the parameters of the freeze foaming process have been

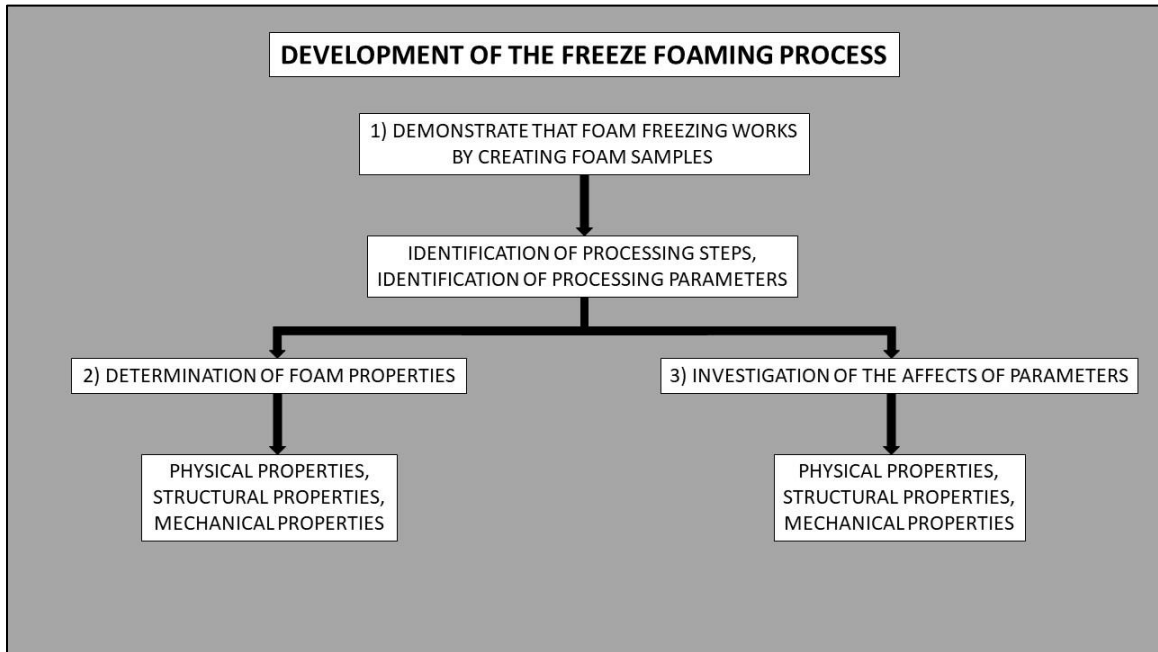


Figure 20. The progress tree needed to meet the research objectives. The second and third objectives can be done simultaneously, but only after the first objective is met.

identified, how they affect the foam can be determined. By isolating the parameters and varying them independently the parameters will be examined. To determine the effects of individual parameters after the foams have been made the structural, physical properties, and mechanical properties will be observed. The research objective has been formed into a diagram shown in Figure 20.

EXPERIMENTAL PROCEDURE

Materials

For this study, Alcoa A-16 aluminum oxide powder was used. Alumina (Almatis, Leetsdale, Pa) was chosen because the sintering characteristics have been well observed and alumina is heavily used in industry. Furthermore, the application of alumina foams in thermal insulation and catalyst supports is a strong driver for the selection. The properties of alumina are provided in Table 2, but those values are given as ranges. For the entirety of the research a density of 3.95 g/cc was used for aluminum oxide. Also, an elastic modulus of 367 GPa and compressive strength of 690 MPa were utilized as baseline bulk values, however, these can be scaled depending upon actual test values as needed.

Aqueous slurries comprised of only four total ingredients; aluminum oxide, deionized water, ceramic dispersant, and a ceramic binder. Deionized water was implemented to ensure consistency and to make sure that the ions in tap water did not impair the aqueous slurries. Darvan C-N (R.T. Vanderbilt Co., Norwalk, CT) was used as a ceramic dispersant. It is a mixture of 25 weight percent ammonium polymethacrylate dispersed into water (39). The ceramic binder used was Rhoplex HA-12 (Rohm & Hass, Spring House, Pa). Rhoplex HA-12 is an aqueous acrylic emulsion that has a solids loading of roughly 45%. The specifics of HA-12 are trade secrets held by Rhoplex. The performance of Rhoplex HA-12 decreases when high shear is applied to it. Therefore, it can only be stirred into a mixture and should not be ball milled as is done with particle

dispersion (40). The binder is required to hold the ceramic particles together prior to high temperature sintering as with more traditional ceramic processing.

Freeze Foaming

Slurry Preparation

Slurry was prepared by traditional ball milling in a HDPE container for 24 hours at room temperature. Water, powder, and Darvan C-N (added at 1.5 wt% of alumina content) was mixed utilizing zirconium oxide milling media to obtain a uniformly dispersed slurry. After dispersion the slurry was separated from the milling media and the Rhoplex HA-12 binder mixed in by hand at low shear to mitigate damage to the emulsion binder system. The amount of water, aluminum oxide, and Rhoplex HA-12 binder put into the slurry was determined using Equation 10 based on the changing parameters of the study in which the amount of alumina was preset. Then the amount of water, dispersant, and binder were solved for to alter conditions for casting. Solids loading is the ratio of alumina to the total volume of the slurry. The m stands for mass of the given term while ρ stands for density.

Equation 10

$$SL = \frac{\frac{m_{Al2O3}}{\rho_{Al2O3}}}{\frac{m_{Al2O3}}{\rho_{Al2O3}} + \frac{m_{H2O}}{\rho_{H2O}} + \frac{m_{HA-12}}{\rho_{HA-12}}}$$

Ball Milling

Ball milling was performed to create a homogeneous slurry. The process involved mixing the aqueous based slurry with milling media and rotating the mixture. The ball milling media consisted of varying sizes of cylinders, spheres, and egg shaped “marbles” made of fully densified aluminum oxide. The speed of rotation for ball millings was set such that the media fell from the top of the container, and smashed the mixture on each rotation. Figure 21 shows the ball milling process. Ball milling was performed for 24 hours to ensure a complete mixture.

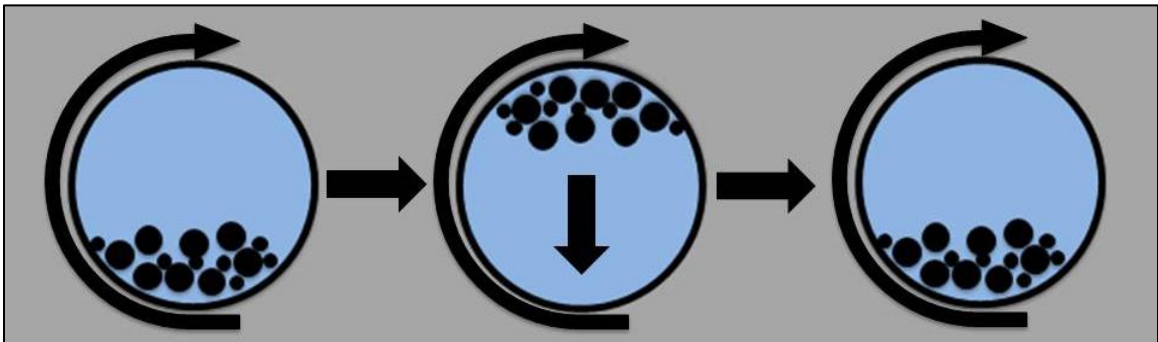


Figure 21. The process of ball milling is depicted, where the milling media reaches the top of the container and then falls to the bottom due momentum and gravity.

Bubble Formation and Simultaneous Freezing

Bubble formation and simultaneous freezing is the heart of freeze foaming. In this step the pores of the foam were made and then set into place using one piece of equipment, a vacuum freeze dryer. The slurry was placed into a mold, which was placed into the vacuum freeze dryer, and the pressure in the freeze dryer was reduced using a traditional rotary vane vacuum pump. The pressure difference of the air within in the slurry and surrounding environment caused the air to expand, forming bubbles. The

bubbles filled the mold and eventually reached a state of equilibrium where expansion stopped. The sample plate holder was set to -30°C which froze the samples.

Once the foam was frozen, and still under vacuum, the temperature of the plate in the vacuum freeze dryer was increased to 30°C to more rapidly drive sublimation.

Sublimation, the process of transforming from solid phase to gas phase while bypassing the liquid phase, was done to remove the water in the foam. The sublimation process was performed for 18 hours to ensure that all of the water was removed from the system.

Once sublimated, the only components left in the foam were the ceramic binder and the aluminum oxide. The Virtis EL-85 vacuum freeze dryer system (Virtis, Gardiner, NY) is depicted in Figure 22.



Figure 22. The shelf type vacuum freeze dryer system (Virtis EL-85) is shown. In the bottom left the vacuum pump can be seen.

Sintering

The foam samples were sintered using electrical resistance box furnaces. Due to limitations in the furnaces available the foam had to be heat treated twice in two separate furnaces. In the first heat treatment the binder and organic additives were removed through thermal decomposition. While in the second sintering, the aluminum oxide was fully densified at significantly higher temperature. In the first thermal treatment the cast foam was heated to 150°C at a rate of 5°C/min. Then the heating rate was decreased to 2°C/min until the temperature was 400°C. At 400°C, the temperature was held constant for 1 hour. The slow heating rate and dwell at 400°C allowed for the binder in the foam to be thermally decomposed out of the foam without damaging it. Then the samples were heated to 1100°C at a heating rate of 5°C/min. The samples were held at 1100°C for one hour. Allowing the foams to densify slightly and increase their strength so that they could be transported from the low temperature furnace to the high temperature furnace. After slightly densifying, the foam was cooled at a rate of 10°C/min back to room temperature. In the high temperature furnace run the aluminum oxide foams were heated at a rate of 5°C/min to 1500°C, where it dwelled for 2 hours. This allowed for the aluminum oxide particles to densify. Then the foam was cooled back to room temperature at a rate of 10°C. Figure 23, shows a graph of the sintering profile.

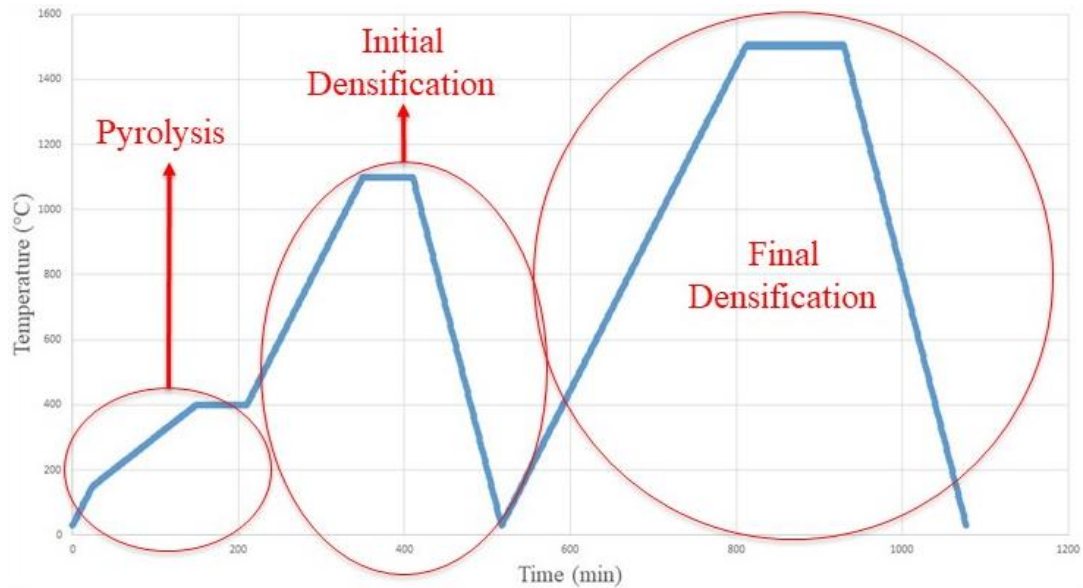


Figure 23. The sintering profile used for all of the foam samples is shown. The sintering profile could be shortened significantly with the use of a two stage furnace capable of high enough temperatures, while being able to stay at low temperatures for an extended period of time.

Parameter Identification

There are multiple parameters that could affect the structure and material properties of the foam produced by freeze foaming. Many of the parameters involve changes to the composition of the slurry.

Solids Loading

The first parameter investigated was the solids loading, related to the amount of ceramic in the slurry on a volumetric basis. Based off of Equation 10, the solids loading was altered over a large range from 60% solids loading to 2.5% solids loading with slurries prepared every 10%, with the exception of 5% and 2.5%. For this study, shown in Table 3, the binder concentration was held at the same value and the same material was

Table 3. The sample parameters for the solids loading study. Where the value in parenthesis is the apparent solids loading after the expansion of the foam had taken place.

Solids Loading Study			
Sample	Percent Solid Loading	Binder Concentration	Foam Volume Expansion Ratio
1	2.5 (0.33)	0.2	7.6
2	5 (0.66)	0.2	7.6
3	10 (1.32)	0.2	7.6
4	20 (2.08)	0.2	9.6
5	30 (3.13)	0.2	9.6
6	40 (4.17)	0.2	9.6
7	50 (5.21)	0.2	9.6
8	60 (6.25)	0.2	9.6

used for the study, aluminum oxide. The foam volume expansion ratio was held at the same value, but at the lower solids loading it was slightly decreased. The foam volume expansion ratio was determined by finding the ratio of the volume of the ceramic slurry and the volume of the foam after foaming

Binder Concentration

The effect of binder concentration was examined related to the amount of binder on a weight percent basis to the ceramic powder content. Binder concentration is the ratio of binder weight to aluminum oxide weight. There were three different solids loading levels selected to evaluate how the binder concentration affects the freeze foaming process; 5%, 20% and 30%. The foam volume expansion ratio was held at a constant value of roughly 10. These solids loading concentrations were chosen because the varying level in binder would not have a large effect on the viscosity, due to the high amount of water. Also, it was observed that the foaming process did not form stable foam

Table 4. The sample parameters for the binder concentration study.

Binder Concentration Study			
Sample	Percent Solid Loading	Binder Concentration	Foam Volume Expansion Ratio
9	5 (0.52)	1.0	9.6
10	5 (0.52)	1.5	9.6
11	5 (0.52)	2.0	9.6
12	5 (0.52)	3.0	9.6
13	20 (2.08)	0.5	9.6
14	20 (2.08)	0.75	9.6
15	20 (2.08)	1.0	9.6
16	20 (2.08)	1.25	9.6
17	30 (3.13)	0.3	9.6
18	30 (3.13)	0.4	9.6
19	30 (3.13)	0.5	9.6
20	30 (3.95)	0.6	7.6
21	30 (3.13)	1.13	9.6

below 30% solids loading so it was valuable to see if increased concentrations of binder concentration could extend the potential range of solids loading percentage. Table 4 displays all of the different binder concentrations that were tested.

Foam Volume Expansion Ratio

The foam volume expansion ratio is an important term used in the direct foaming process and was incorporated in the freeze foaming process to provide a validation for the technique. The foam volume expansion ratio is the ratio of the original slurry volume to

Table 5. The sample parameters for the foam volume expansion ratio study.

Foam Volume Expansion Ratio Study			
Sample	Percent Solid Loading	Binder Concentration	Foam Volume Expansion Ratio
22	30 (15.0)	0.3	2
23	30 (7.50)	0.3	4
24	30 (5.00)	0.3	6
25	30 (3.75)	0.3	8
26	30 (3.00)	0.3	10
27	30 (2.00)	0.3	15
28	30 (1.50)	0.3	20

the volume of the expanded foam in the green state. The effects of this parameter were isolated by keeping a constant solids loading of 30% and binder concentration of 30%, while the foam volume expansion ratio was altered from 2 to 20. The different foam volume expansion ratios that were evaluated is presented in Table 5.

Pressure

The pressure that the foaming process took place at was applied in the same each time. The pressure in the vacuum freeze dryer was controlled by opening and closing manually actuated valves. Therefore, the pressure was not directly controlled, but the rate of change in pressure was controlled. The process of changing the pressure within the vacuum freeze dryer was done the same way for each sample. In this manner the liquid slurry was forced to foam to the given volume of the mold as quickly as possible without

exceeding the given volume, by closing the valve slightly. Then the valve was held at a constant position until the foam froze.

Density Measurements

One very important property for foam is the density and as shown earlier the mechanical properties can be estimated using the relative density of foam. To evaluate the density measurements, the volume dimensions were measured using digital calipers (General Ultratech, Secaucus, NJ) with a resolution of 0.01mm. Samples were cut out of bulk foam, into cylinders. The samples had a consistent diameter of 19mm and varying heights. The tops and bottoms were flattened by cutting them using a razor blade. The mass was measured using a Sartorius CPA225D digital scale (Sartorius, Gottingen, Germany) with a resolution of 0.00001g. After all the necessary measurements were taken density and relative density were determined using Equation 11 and Equation 2. In Equation 1, ρ stands for density, while m stands for mass, and V stands for volume.

Equation 11

$$\rho = \frac{m}{V}$$

Microstructure

To characterize both the macrostructure and microstructure of the foam samples imaging using light microscopy was utilized given the macro scale of the cell sizes. The structure was analyzed using an Olympus BX41 light microscope (Olympus, Center Valley, PA). The microscope can be seen in Figure 24. Dark field microscopy was

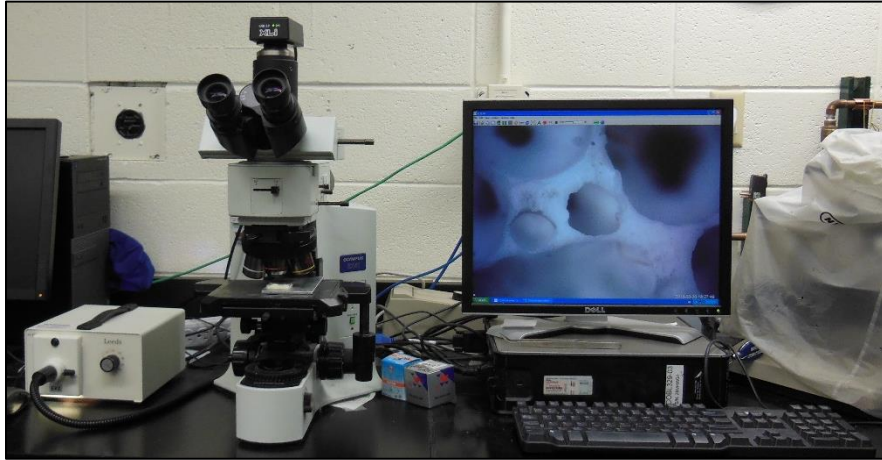


Figure 24. The Olympus BX41 light microscope utilized, with capability to 1000x.

performed and samples were examined at different magnifications from 50x to 1000x. Before imaging the samples were filled with fast curing mounting epoxy (Ted Pella, Redding, CA) and cut into 4.5 mm thick sections to expose the cross section of the foam. After cutting, the samples were sanded with 1200 grit sand paper and then polished with a felt pad. After getting images, Equation 3 was utilized to determine the relative density.

Compression Testing

The mechanical properties of the foam were analyzed by performing compression testing. While there is a standard testing procedure for honeycomb structures, but there is no standard for compression testing of brittle foams (12, 20). To alleviate stress concentration on the ceramic foam samples one end of the sample was capped with epoxy and had a compliant layer of silicon pressing on the other end. This method has been shown to create much cleaner test results (12) in low density foams. To ensure consistency between samples, samples were cut from bulk foam to cylinders of 19 mm diameters and roughly 17 mm heights. Then fast curing mounting epoxy (Ted Pella,

Redding, CA) was applied to the bottom of each sample to create smooth a surface. After the epoxy had cured the upper surface of the sample was flattened using a razor blade so that the upper and bottom surfaces were parallel. The testing was done using an Instron 5543 (Instron, Norwood, MA) at a rate of 1mm/min. The sample holders were machined from aluminum and had a diameter of 25.4 mm. Figure 25, shows the system used for compression with a sample loaded into it. The sample holders were machined so that they self-aligned. The sample holder was machined so that even if the sample was not flat the loading fixture would tilt and apply the load evenly over the surface. Figure 25, illustrates this feature while showing the compliant silicon layer and bottom epoxy layer.

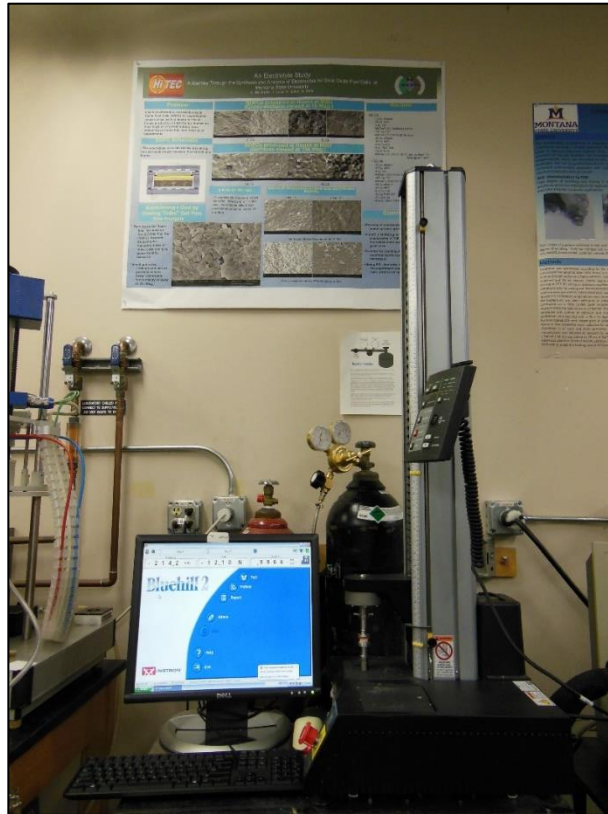


Figure 25. Compression testing was done on a table top Instron. The maximum load that can be applied for this Instron is 1kN.



Figure 26. The compression test set up is shown. The metallic ball aligns the loading plate. The compliant silicon layer can be seen in orange, while the lower epoxy layer can be seen touching the support plate.

RESULTS AND DISCUSSION

Casting Parameters

Freeze foaming has a fairly large variability in formula parameters that will result in a foam providing excellent tailor-ability of the process. Trials from the solids loading study identified, that with a binder concentration at 0.3 and a foam volume expansion ratio around 10, with a solids loading from 30% to 50% allowed for the formation of a solid foam. Above the 50% solids loading, the solution was excessively viscous to ball mill, for the given binder content. At 20% solids loading a foam was shown to form, however during freezing the bubbles collapsed. Both the binder concentration and viscosity were too low and right when the bubbles were forming the effects of drainage became active and the bubbles collapsed due to thinning of the bubble walls. Below a solids loading of 20% bubbles were not stable and would collapse upon formation. The results of the solids loading study can be seen below in Figure 27.

Foam samples of 5%, 20%, and 30% solids loading were synthesized at different binder concentrations to evaluate the effects the binder has on the foaming process. It should be noted that the acrylic emulsion binder is not water soluble so the general behavior of water is not being modified as would a soluble binder such as PVA, PEG, or PPG. It was found that for a solids loading of 30% that the binder concentration ranging from 0.3 to the maximum possible concentration of 1.13, above 1.13 the solids loading would increase as well, allowed for the formation of stable foam. For foam samples with a solids loading of 20% it was found that the binder concentration could range from 0.75



Figure 27. Results of the solids loading study, where the sample numbers correlate with Table 3. All of the samples are shown in the green state prior to high temperature sintering.

to 1.25 but below 0.75 a stable foam could not be formed. Lastly, a binder concentration at or above 2.0 was able to form a stable foam with a solids loading of only 5%. However upon sintering the foam structure collapse. The results of the binder concentration study can be seen in Figure 28 and Figure 29.

The last parameter explored was the foam volume expansion ratio. It was found that the expansion ratio can vary from 2 to 15 while forming a stable foam that could be sintered. While a green state foam with an expansion ratio of 20 could be made, it did collapse upon sintering. It was found that as the foam volume expansion ratio increased the variation in pore size increased. The results of the foam volume expansion ratio study can be seen in Figure 30.



Figure 28. Results of the binder concentration study for 5% and 20% solids loading, where the sample numbers correlate with Table 4. All of the samples are in the green state prior to high temperature sintering.

The results from the parameter variation studies leads to some important insights about the freeze foaming process and suitable processing formulations for freeze foaming. First, for the bubbles to form the use of a binder is necessary. During regular de-airing of ceramic slurries, without binder, the air escapes and causes the slurry to appear as if it boiling. If there is a ceramic binder in the slurry the de-airing process is very different. As seen in the standard de-airing process, and freeze foaming process, as the pressure drops in the vacuum freeze dryer the pressure difference of the air within in the slurry and surrounding environment causes the air to expand, forming bubbles, but HA-12 adds some plasticity to the bubbles, causing them to be able to stretch and withstand variations in pressure. Then the bubbles fill the mold and eventually reach a



Figure 29. Results of the binder concentration study for 30% solids loading, where the sample numbers correlate with Table 4. All of the samples are in the green state prior to high temperature sintering.

state of equilibrium where expansion stops. In addition, the use of an acrylic emulsion is very important. Due to the fact that the acrylic emulsion is non-water soluble, by definition, it does not interfere with the freezing properties of water. This process is shown in Figure 31. Second, the ceramic slurry must have a high enough concentration of binder. The interaction between the acrylic particles in the slurry allows for bubbles to form, but to ensure that bubbles will form during the freeze foaming process a minimum threshold must be met. Then bubbles will form at any concentration above this point. The binder concentration must be high enough that the binder has an interconnected network

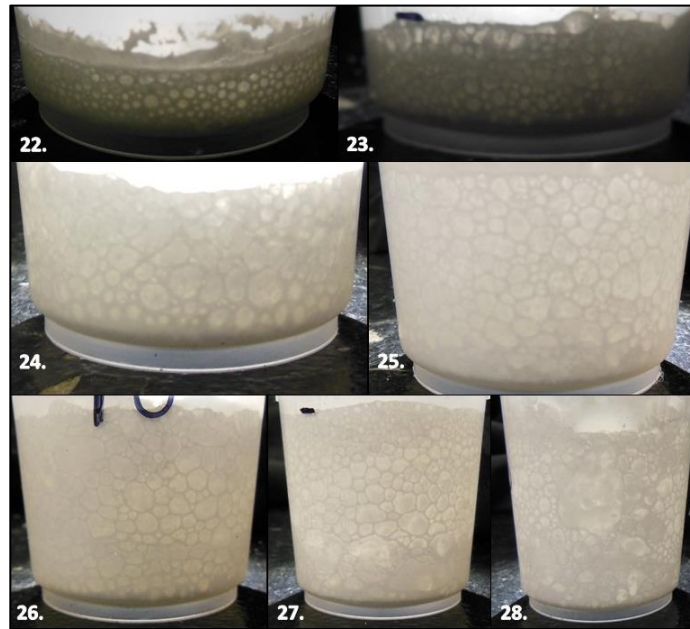


Figure 30. Results of the foam volume expansion ratio study for 30% solids loading with 30% binder concentration, where the sample numbers correlate with Table 5. All of the samples are in the green state.

throughout the ceramic slurry or the binder will not be able to allow for bubbles to begin growing. Third, the ceramic slurry needs to have a high enough viscosity. The viscosity of the slurry must be high enough to ensure that the walls and plateau borders in the bubbles do not get too thin. When the bubbles grew too thin they collapsed, because the liquid on the walls of the bubble stretch to the point that any interactions between different particles cannot take place. Even though the bubbles in the freeze foaming process are only liquid for a short time before they become frozen, the effects of drainage must be limited. Surfactants help limit drainage by adsorbing at the air-water interfaces in the foam limiting the mobility of liquid, but higher viscosity fluid does too this can be seen in Equation 1, where the viscosity term is in the denominator of the PDE. Although the viscosity levels were not measure directly it is known that the viscosity increases with

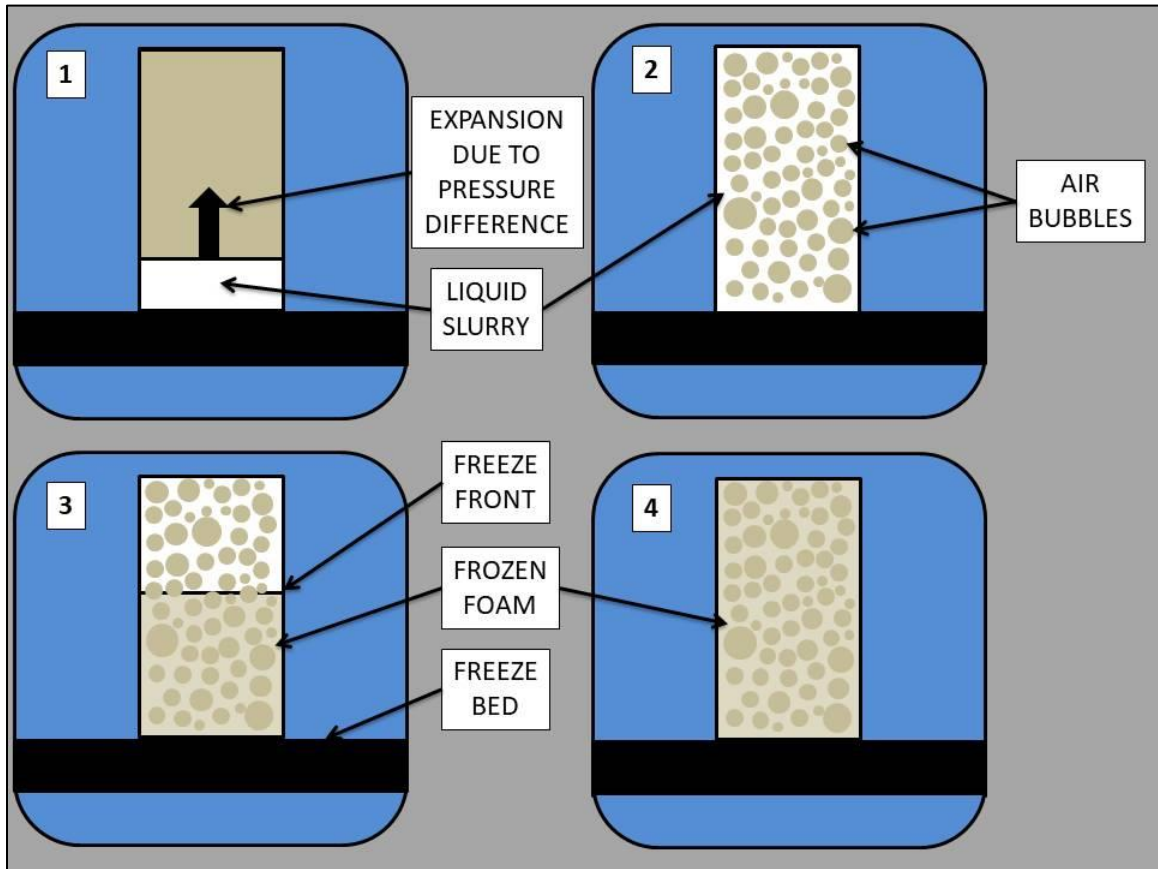


Figure 31. The bubble formation and freezing step are shown. Image 1 shows the slurry and mold in the vacuum freeze dryer when expansion starts to take place. Image 2 shows the formed bubbles and liquid slurry before freezing takes place. Image 3 shows the foam part way through the freezing process. Image 4 shows the formed frozen foam.

solids loading and higher binder concentrations. If the bubbles thin out too much during the foaming process they would burst while freezing. Lastly, the ceramic particles cannot get spread too far apart during the foaming or freezing step. If those three criteria are met the Freeze foaming process will yield green foam structure as the process in Figure 30 shows. This can happen in two different ways first the slurry can begin with too few particles in the slurry by having too low of a solids loading. The other way is during the foaming process the foam can be too spread apart. Due to too high of foam volume expansion ratio. In either situation even if a foam can make it through the sublimation

process, particles will not be able to sinter together because the particles are too far apart and unable to overcome the activation energy necessary to start sintering.

There is one parameter that was not altered due to system limitations, but it was identified and the effects of it can be estimated. The effect of cooling rate was not investigated. During the foaming and freezing process, the freeze bed in the vacuum freeze dryer was set to the same value. This parameter was not investigated, because the system would not be able to impact the structure of the ice. The freeze bed can reach to a temperature of roughly -90°C , but to cause amorphous ice it would need to be able to achieve a temperature around -130°C (31). By decreasing the temperature of the vacuum freeze dryer the effects of drainage could be limited, because the amount of time that the foam is a liquid would decrease. Second, the effects of mold shape and design were not examined.

Physical and Structural Properties

Examining the results from the processing variation changes in the physical properties of various foam samples it was determined that freeze foaming

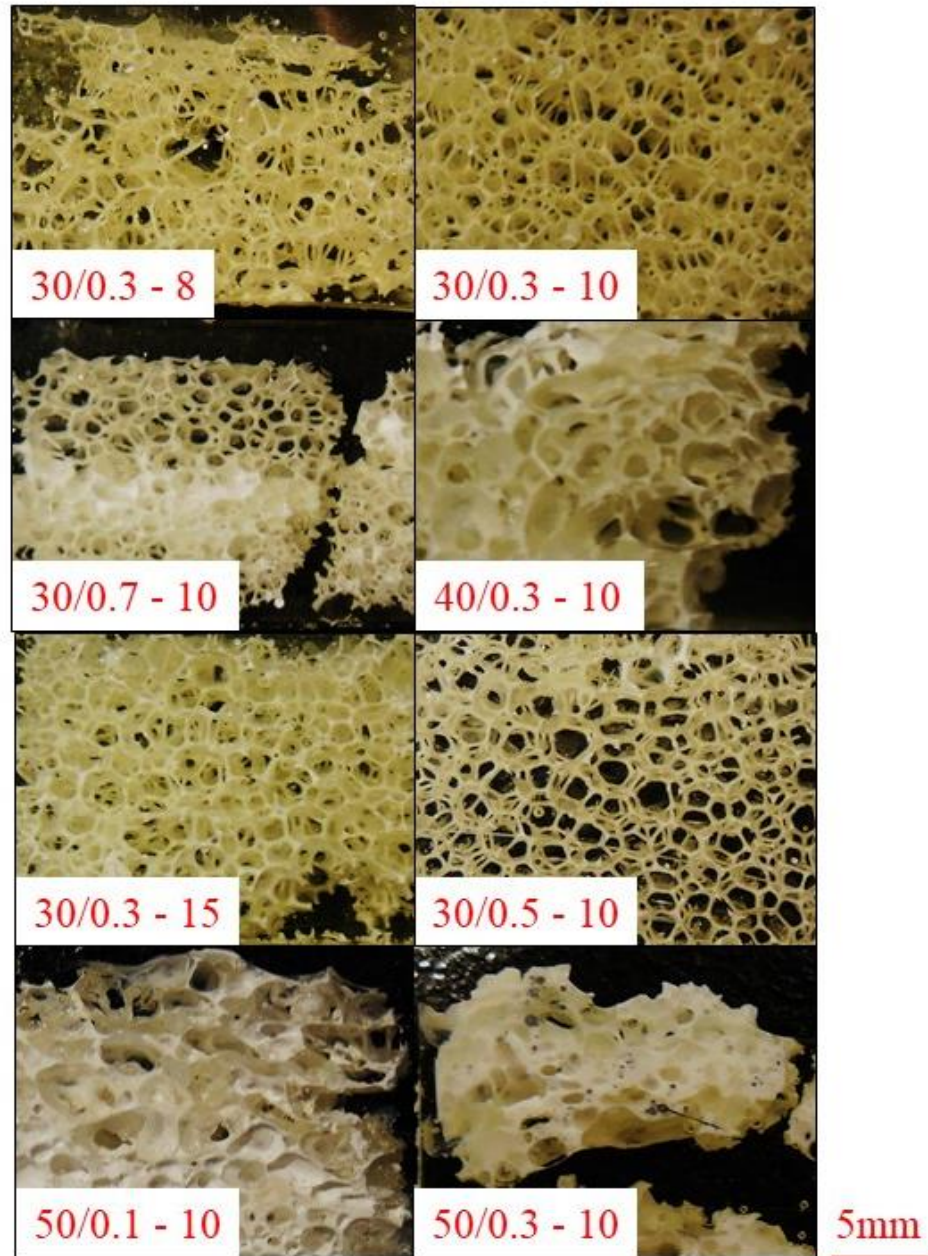


Figure 32. The different processing parameters yielded different types of foam ranging from extremely porous open cell foam to a mixed cell foam.

yielded consistently high levels of porosity with large pores. In addition, binder concentration, solids loading, and foam volume expansion ratio all affect porosity, pore size and even foam type.

Looking at the cross sections of various foam samples it can be seen that the structure varies drastically with alterations to the different processing parameters. In fact, the foam transitions from an extremely porous open cell foam to a mixed cell foam. Figure 32 shows the different types of foam synthesized using freeze foaming.

As the binder concentration increases the porosity level decreases. For a foam with a solids loading of 30%, a binder concentration of 0.3, and a foam volume expansion ratio of 10 a porosity of 93.9% was achieved. With the binder concentration increased to 0.5 the porosity dropped to 90.7% and the porosity decreased to 90.2% when the binder concentration was raised to 0.7. In addition with an increase in binder concentration the pore size also decreases. There is an increase in the number of small pores while large pores are still formed. This suggests that higher binder concentrations reduces the effects of coarsening. The average pore diameter achieved was 1487 μm , 1359 μm , and 1142 μm for binder concentration of 0.3, 0.5, and 0.7. Figure 33 and Figure 34 show the changes in porosity and pore size with changes in binder concentration.

Similarly for solids loading the same relationship is seen, but the affect is more impactful. The porosity of the foam decreases from 93.9% to 91.1% and then 58.8% as the solids loading increases from 30% to 40% and up to 50%. Also, the pore size decreases with increased solids loading. At solids loadings of 30%, 40% and 50% the pore

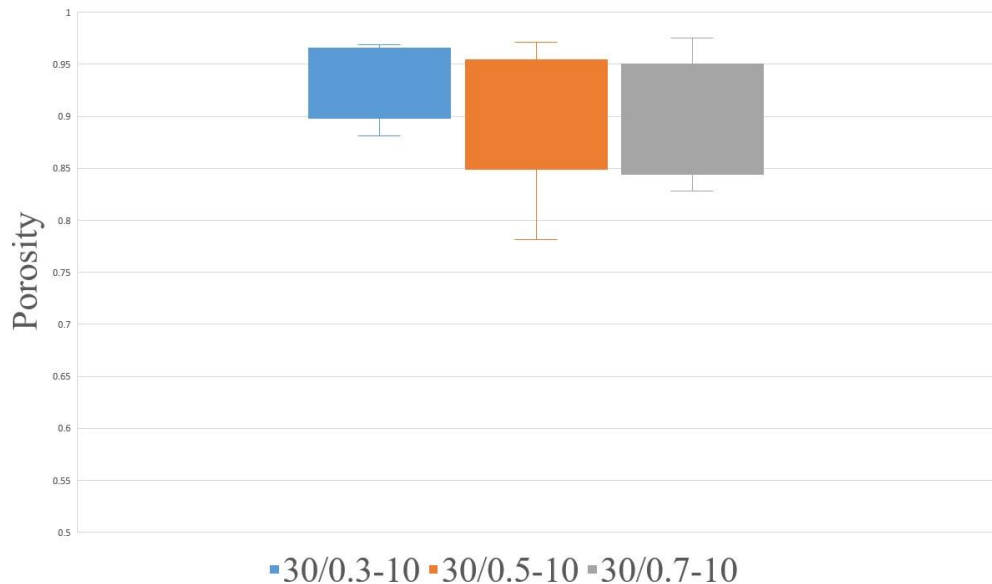


Figure 33. Porosity as a function of binder concentration. All of the samples had a solids loading of 30% and a foam volume expansion ratio of 10. The average porosity decreases from 93.9% to 90.7% and 90.2% while binder concentration increases from 0.3 to 0.5 and 0.7.

sizes are 1487 μm , 1112 μm , and 578 μm respectively. These results can be seen in Figure 35 and Figure 36 that show the impact in variation of the solids loading.

Additionally, it was observed that as the foam volume expansion ratio increases a peak porosity value is reached and where it plateaus. Foam with a foam volume expansion ratio of 8 was observed to have a porosity of 85.3%. The porosity peaked at a value of 93.9% with a foam volume expansion ratio of 10. Then the porosity decreased to 89.8% when the foam volume expansion ratio increased to 15. The same pore size followed the same pattern where the average pore size was to be 1005 μm , 1487 μm , and 1118 μm for foam volume expansion ratios of 8, 10, and 15. Figure 37 and Figure 38 show the relationships of pore size and porosity versus foam volume expansion ratio.

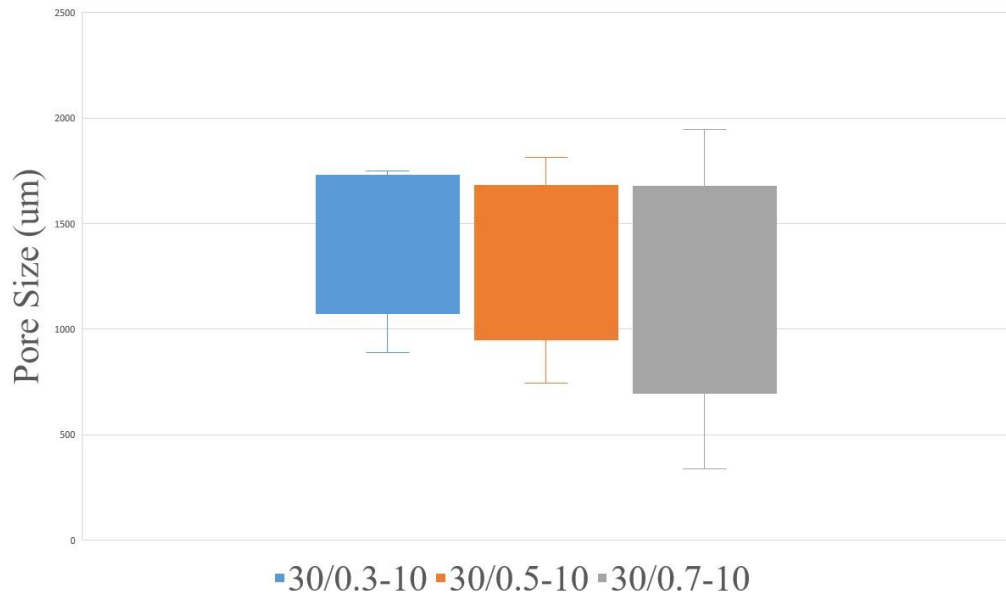


Figure 34. Pore size as a function of binder concentration. The pore size decreases from 1487 μm to 1359 μm and 1142 μm as the binder concentration increases from 0.3 to 0.5 and 0.7. All of the samples had a solids loading of 30% and a foam volume expansion ratio of 10.

Two different techniques were used to determine the porosity of three different foam types. Digital calipers and light microscopy were used to measure the porosity of foam types 30/0.7 – 10, 40/0.3 – 10, and 50/0.1 - 10. These two techniques, although determining two different values for porosity, determined quite similar values of porosity only having a maximum of 7% porosity difference. For all of the foams the caliper method estimated higher porosity than the microscopy method. Figure 39 shows the comparison of the two methods used to determine porosity.

The data from the physical and structural properties shows that to achieve the highest porosity the binder concentration and solids loading should be minimized while a foam volume expansion ratio of 10 should be used. In addition, the data shows that different formulas can lead to different structures. The high range in porosity observed in

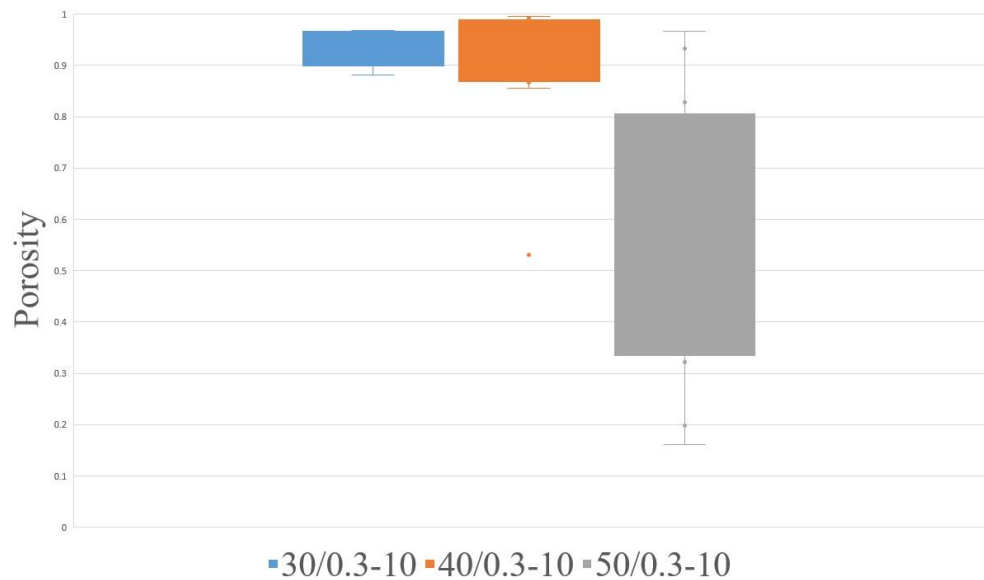


Figure 35. Porosity as a function of solids loading. The porosity decreased from 93.9% to 91.1% with an increase in solids loading from 30% to 40%. Then the porosity dropped to 58.8% to 50% solids loading. The binder concentration and foam volume expansion ratio were held constant at 0.3 and 10.

different foam types suggests that by altering casting parameters the foam can be tailored easily. This highly advantageous capability means that by altering the solids loading, binder concentration, and foam expansion volume ratio that the structure of the foam can be altered. By altering the structural properties other properties, like mechanical properties, can also be manipulated as well. The average pore size of the foams, made through freeze foaming, ranges from 578 μm to 1487 μm , while the smallest pore size achieved was 140 μm and the maximum pore size achieved was 2126 μm . The porosity levels achieved ranged from 59% to 94%.

By comparing the porosity ranges and pore sizes achieved by freeze foaming to the traditional processes it is seen that freeze foaming is comparable. Freeze foaming is shown to even achieve porosity levels higher than that seen in direct foaming and replica

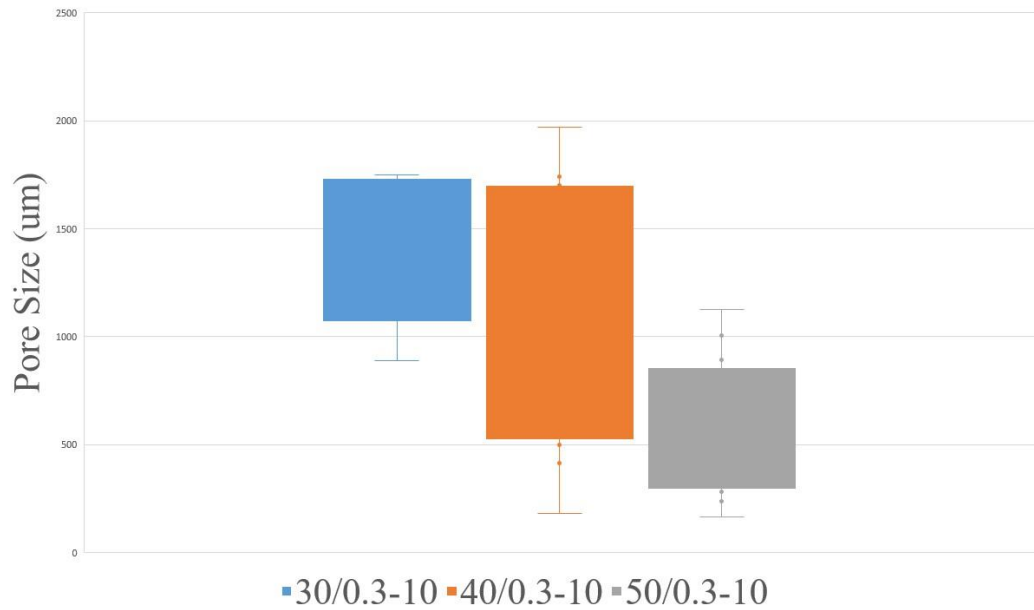


Figure 36. Pore size as a function of solids loading. The average pore size dropped from 1487 μm , 1112 μm , and 578 μm respectively at solids loadings of 30%, 40% and 50%. Each sample had a binder concentration of 0.3 and a foam volume expansion ratio of 10.

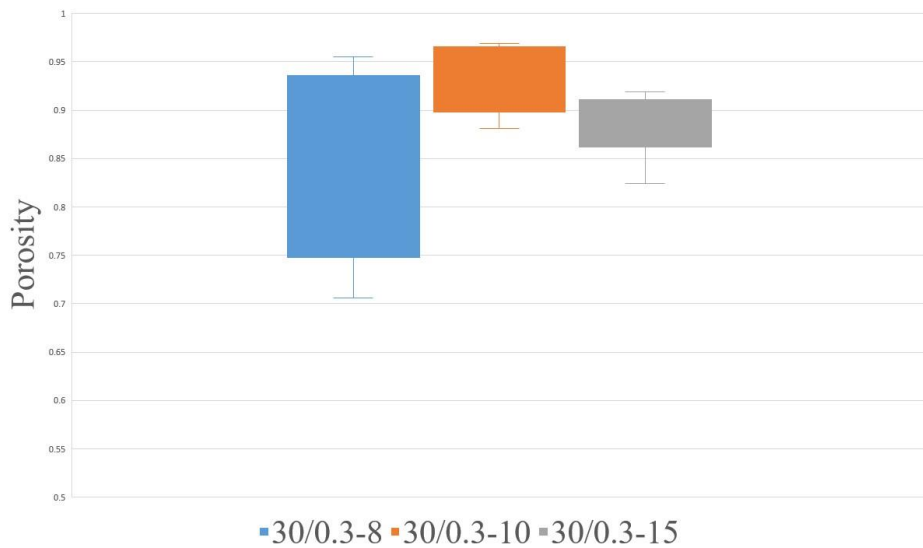


Figure 37. Porosity as a function of foam volume expansion ratio. All of the samples had a solids loading of 30% and a binder concentration of 0.3. The porosity peaked at 93.9% with a foam volume expansion ratio of 10 from a porosity of 85.3% at an expansion ratio of 8. Then the porosity decreased to 89.8% porosity at an expansion ratio of 15.

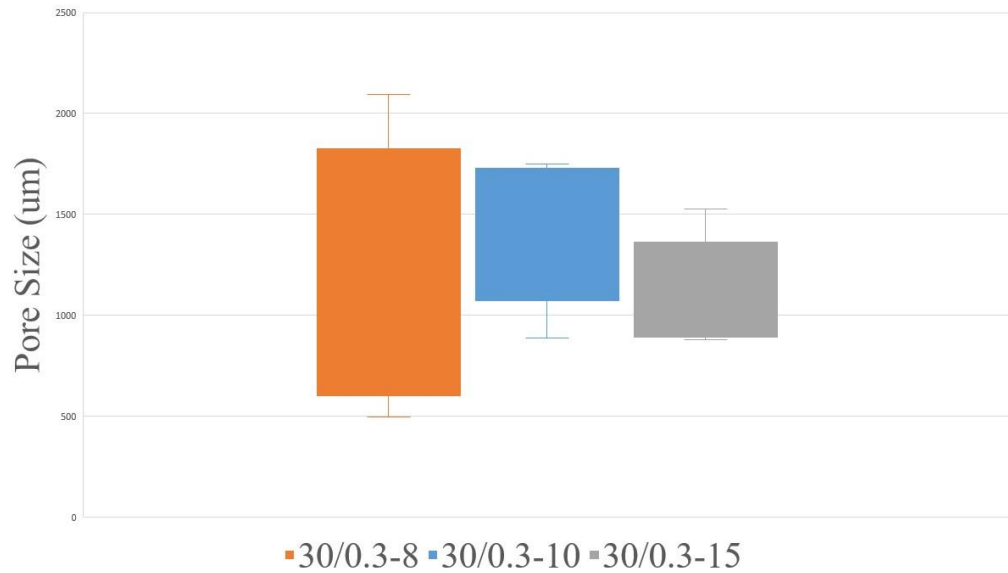


Figure 38. Pore size as a foam volume expansion ratio. The average pore size goes from 1005 μm to 1487 μm , and 1118 μm respectively at expansion ratios of 8, 10, and 15. Each sample had a binder concentration of 0.3 and a solids loading of 30%.

templating. In addition the achievable pore sizes for freeze foaming is lower than replica templating and higher than both direct foaming and sacrificial templating. The comparison of freeze foaming to traditional techniques is shown in Table 6.

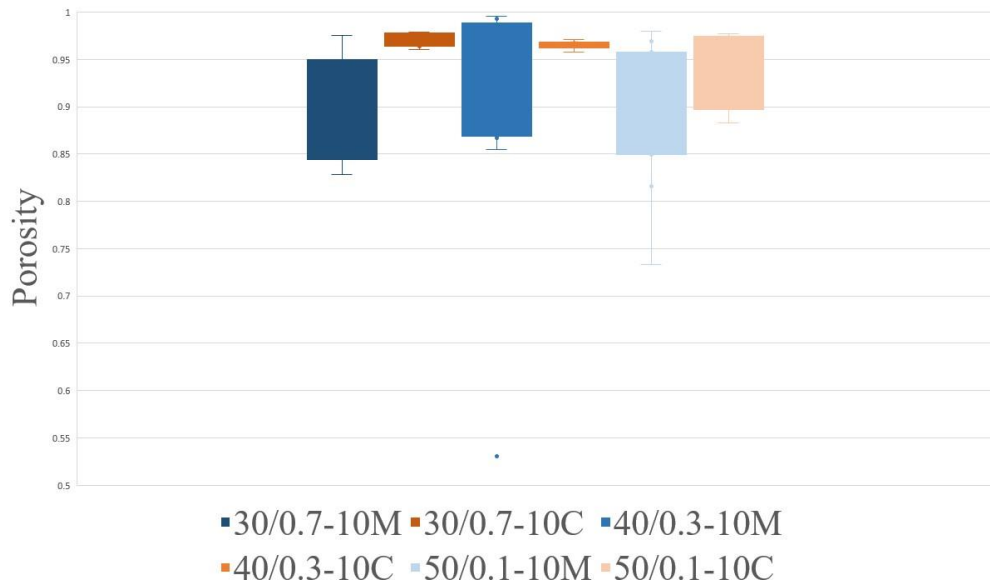


Figure 39. The difference in porosity measurements for microscopy measurements and caliper measurements. The largest difference between the two methods was at 30% solids loading. There was a 7% difference.

Table 6. The porosity and pore size ranges of freeze foaming are compared to the traditional synthesizing technique (24).

Comparison of Synthesis Techniques		
Synthesis Technique	Porosity	Pore Size
Freeze Foaming	59% - 94%	140 μm - 2.1 mm
Direct Foaming	up to 93%	35 μm - 1.2 mm
Sacrificial Templating	up to 90%	1 μm - 0.7 mm
Replica Templating	40% - 95%	200 μm - 3.0 mm

Mechanical Properties

Compression testing allowed for the mechanical properties of various foam samples to be tested. Figure 40 shows the typical testing results for compression testing. The foam samples that had a solids loading of 50% had two distinct test results. Half of the samples had very low strength and moduli, while the other half had drastically higher mechanical properties.

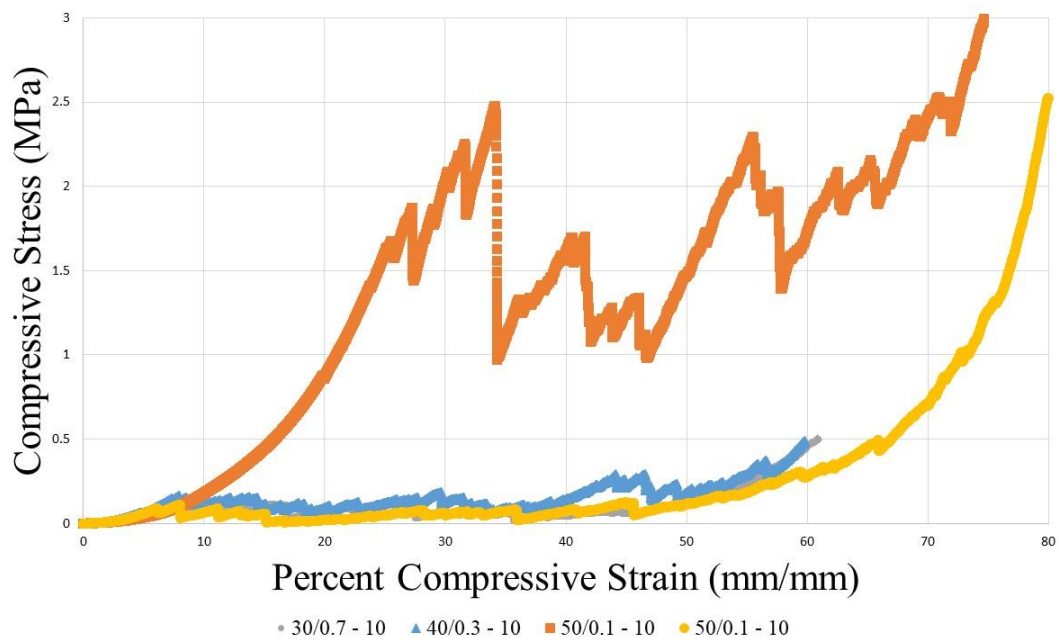


Figure 40. Typical test results for the different foam sample types tested through compression testing. The 50/0.1 – 10 foam had two distinct types of test results. Half of the samples had very high strength while half had very low strength. They also had substantially different relative densities.

The compression test can be broken down into four different sections. The first section is where the compliant layer compressed. The second section is where the actual foam began compressing before it failed. In this section the elastic modulus was



Figure 41. The effects of progressive failure resulted in ceramic foam chips flying off of samples during compression testing.

determined by taking the slope of line right before the maximum local peak. Also, the compressive strength was found by taking the local maximum peak value. In section three progressive failure occurred, as is common with ceramics in compression (38).

Cracks would propagate through the struts of the foam causing chipping. Figure 41 shows how progressive failure occurred in the foam samples and provides validation of the progressive mode of failure observed in the stress-strain plots. The numerous ceramic foam flakes shown in the figure accumulated on the Instron during just one compression test. In addition, in the compression test results where large drops occurred

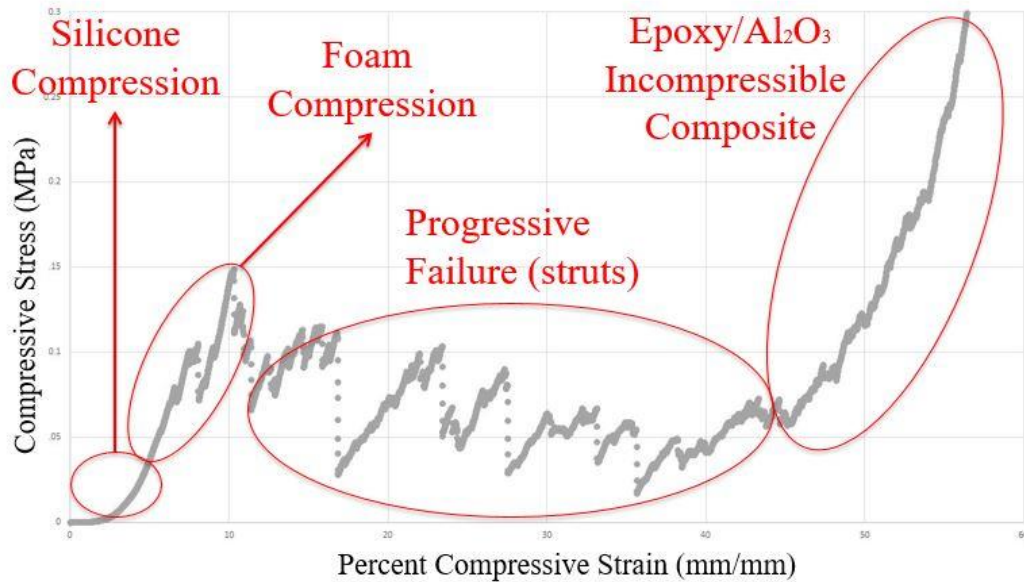


Figure 42. The four sections of the compression test are highlighted. Section one is where the compliant silicon layer is compressing, section two is where compression of the foam begins until the first failure begins, section three is where progressive failure occurs, and section four is where the epoxy-aluminum oxide composite begins being compressed.

instantaneously there was an audible cracking sound and ceramic chip directly observed during the test. This progressive fracture continued all the way through the sample until only the bottom epoxy infiltrated aluminum oxide foam remained intact. In section four, the foam had already chipped all the way down to the epoxy cap and the epoxy-aluminum oxide composite does not compress very much so a very steep peak occurs. These four sections are highlighted in Figure 42.

Progressive failure has been observed in other brittle ceramic material systems. Zhu and Tang (42) looked at the amount of acoustic emissions during compression testing of rock. The results of the compression testing for rock had large drops in stress, just like as observed in the foam samples, and associated with those drops there was spikes in the counts of acoustic emissions. These increased acoustic emissions are

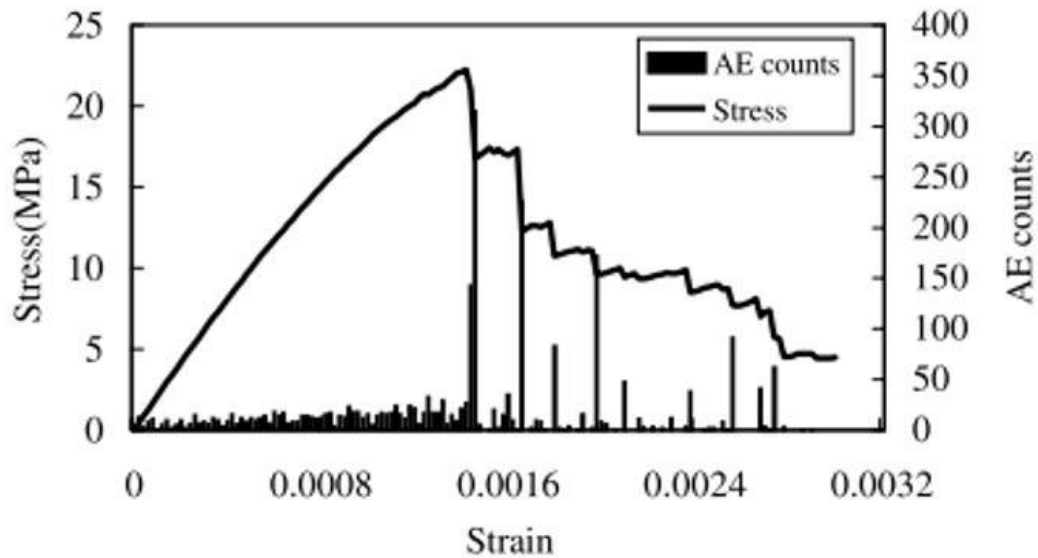


Figure 43. Spikes in acoustic emissions are seen with drops in stress values for compression testing of brittle rock. The acoustic emissions are associated with cracks propagating through the material. This behavior was observed in the ceramic foam samples synthesized using freeze foaming (42).

associated with cracks propagating through the material. The similarity of compression test results shows that the foam behaves in the same manner as other ceramic materials.

Figure 43 shows the compression test results observed by Zhu and Tang.

For foam samples with a solids loading of 30% the average compressive strength is 0.065 MPa. The strength increases to 0.149 MPa with a solids loading of 40%. When the solids loading is increased to 50% the average compressive strength jumps up to 1.06 MPa. The elastic modulus also increases with solids loading from 1.9 MPa to 3.4 MPa and 7.5 MPa with solids loadings of 30%, 40%, and 50%.

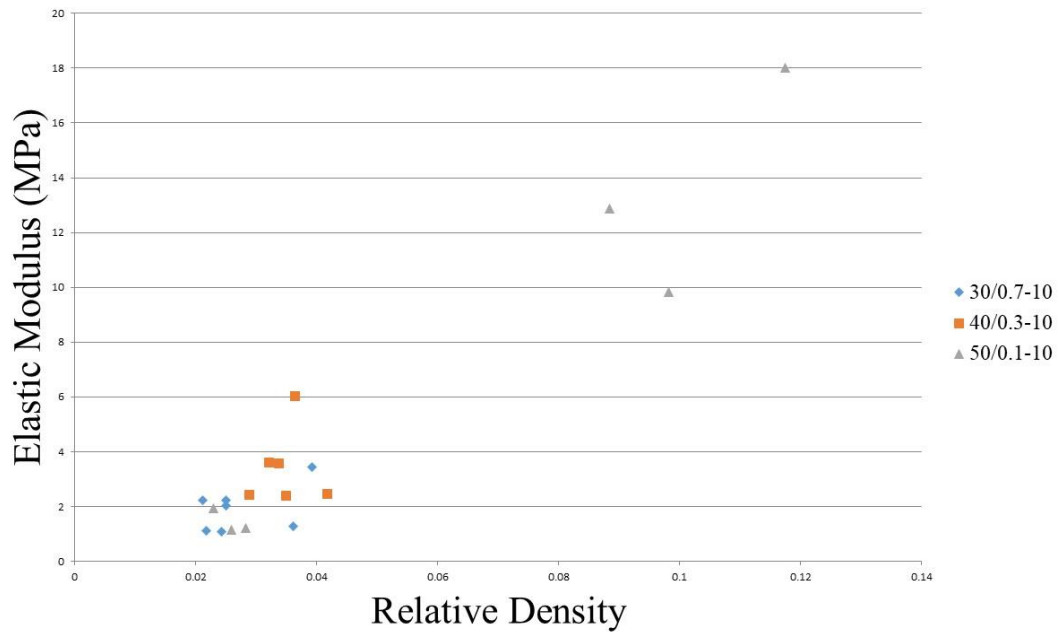


Figure 44. Elastic modulus as a function of relative density is shown. The highest modulus was 18 MPa at porosity of 88.3%.

By comparing the elastic moduli of the foam samples to their respective relative density some patterns can be seen. Figures 45 and 46 show the relationships as well as what the expected elastic modulus should be utilizing Equations 6. Through analysis it can be found that the foam does seem to follow the relationship found by Ashby and Mehl, but with much lower factor than what they had determined. If Equation 6, is adjusted by a factor of 0.01 the relationship of relative density to elastic modulus is squared. Although it is not close to the estimated value from established models. The fact that the foam follows the same squared value as the Ashby and Mehl model indicates that the freeze foaming process yields foams that are comparable to foams manufactured from one of the more traditional manufacturing methods. Equation 12 shows this alteration to the equation and Figure 43 shows how the data fits this curve much better.

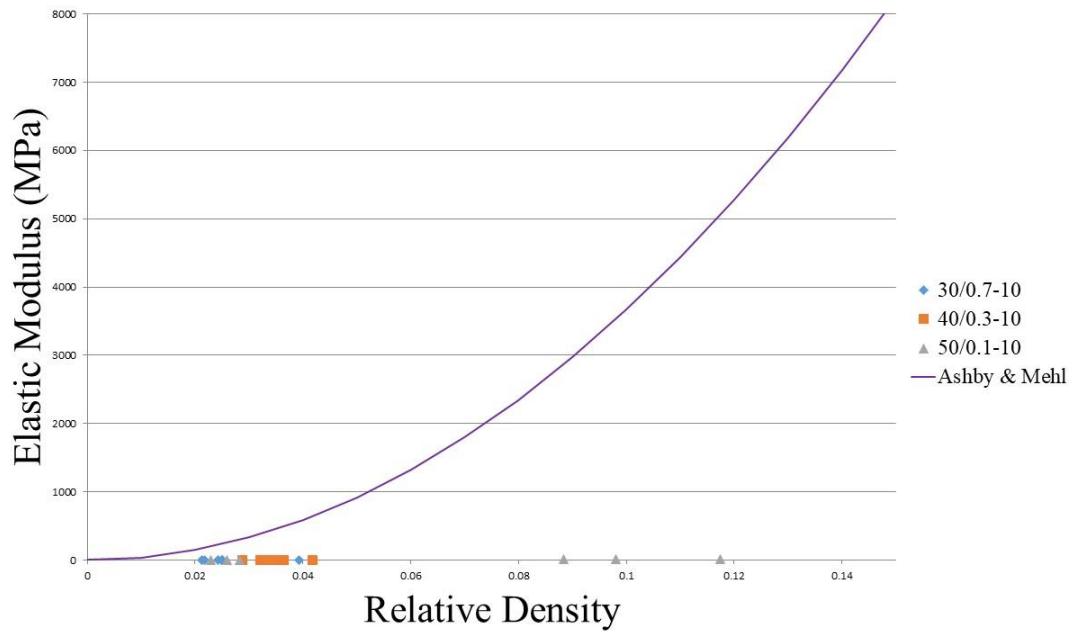


Figure 45. Elastic modulus as a function of relative density is shown with what the expected modulus should be based off of the Ashby and Mehl model.

Equation 12

$$E = 0.01E_S \left(\frac{\rho}{\rho_S} \right)^2$$

This same relationship is observed with regards to compression strength. Where the factor found by Ashby and Mehl, is drastically too high for the results observed. If the factor in Equation 8 is adjusted from 0.65 to 0.065 the samples follow the same power factor of 3/2 that they determined. This necessary adjustment can be seen in Equation 13, while the relationship between compression strength and Equation 13 can be seen in

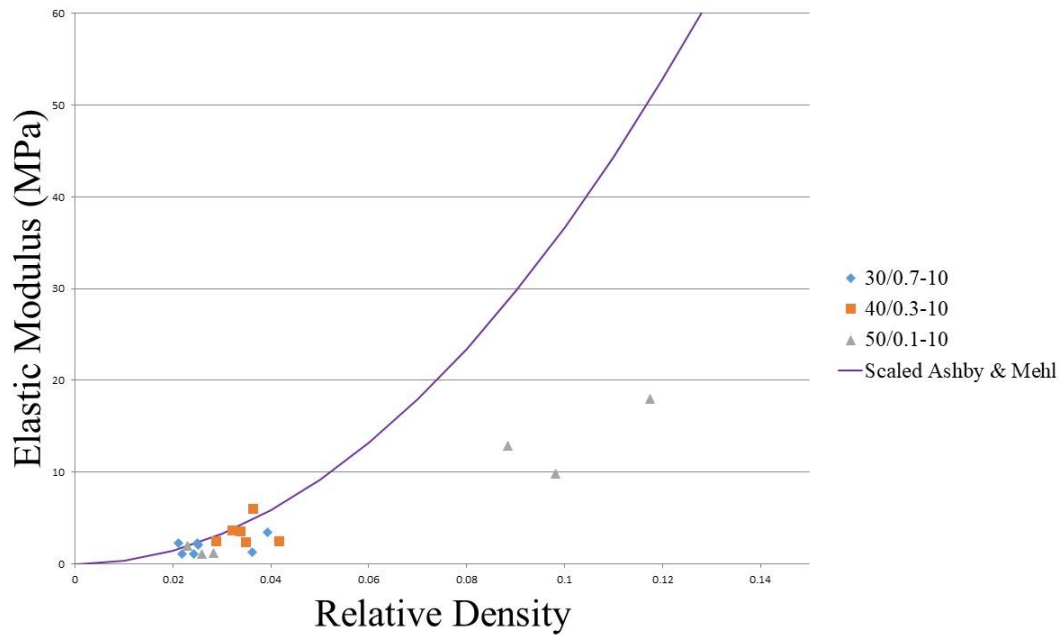


Figure 46. Equation 12 shows a much better fit for elastic modulus as a function of relative density.

Figure 47. In addition, other research groups have found compressive strength of aluminum oxide foam that is much lower than the Ashby and Mehl model and comparable to values of foams made using freeze foaming. Luyten, et al. reported a strength of 8 MPa with a porosity of 75% for aluminum oxide foam made by direct foaming (16). Schumann and San-Miguel found a strength of 6 MPa with a porosity of 83% for aluminum oxide foam synthesized using direct foaming (41). These values are seen in Figure 47, and show that the ceramic foam made through freeze foaming has comparable strength to foams made using direct foaming.

As the structural and physical property analysis suggested the mechanical properties of foam made through freeze foaming are adjustable. By increasing the solids loading of the foam both the elastic modulus and compression strength can be improved.

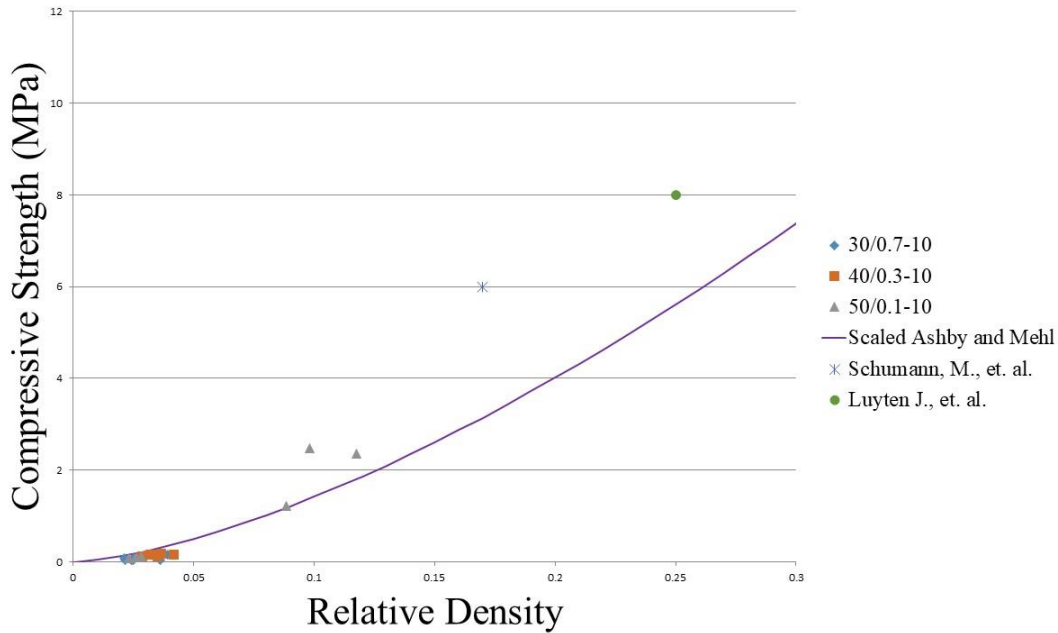


Figure 47. The relationship between compressive strength and relative density shows a comparable trend to the Ashby and Mehl model with a reduction of a factor of ten, Equation 13 (16,41).

In addition, although the factor did need to be adjusted the foam made through freeze foaming did follow the model for ceramic foams that can be seen in the literature. Also, progressive failure was observed through compression testing. This is known to be the mechanism for compressive failure in brittle cellular solids. There is one aspect of the compression data that is abnormal. Looking at the samples of 50/0.1 – 10 foam there is a substantial difference in relative density between samples even though the samples went through the same processing parameters.

Equation 13

$$\sigma_f^* = 0.065 \sigma_f \left(\frac{\rho}{\rho_s} \right)^{3/2}$$

Looking at how the Ashby and Mehl model was developed helps provide insight into why the foam samples tested did not have mechanical properties equivalent to what the Ashby and Mehl model predicts. First, all of the relationships developed, including elastic modulus and compressive strength, were developed using the relationship of relative density (Equation 2). Ashby and Mehl assumed that cellular solids have a repeating structure that is a cube, while the structure observed in the foam consisted of a network of struts in circular, oval, pentagonal, and hexagonal orientation in a spherical configuration. The difference of foam structure between the Ashby and Mehl model and observed structure are shown in Figure 48. The thickness and length of the foam structure used to determine relative density are highlighted. This difference in structure would result in different levels of porosity measurements which impact the estimated mechanical properties.

Second, in the development of both the elastic modulus and compressive strength data was collected from numerous sources. Then Ashby and Mehl plotted the data in a

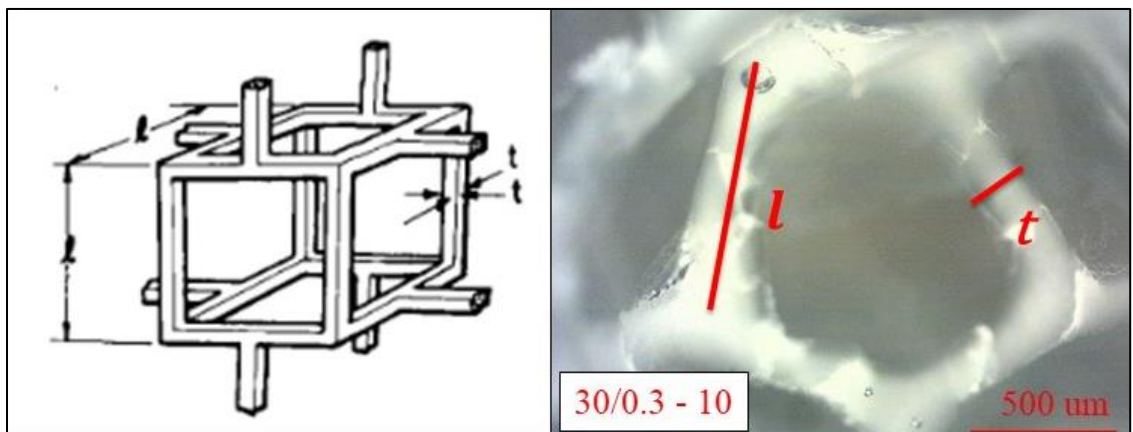


Figure 48. The differences in the Ashby and Mehl model and observed structure of an open cell foam are shown, which impact the relative density and mechanical properties (38).

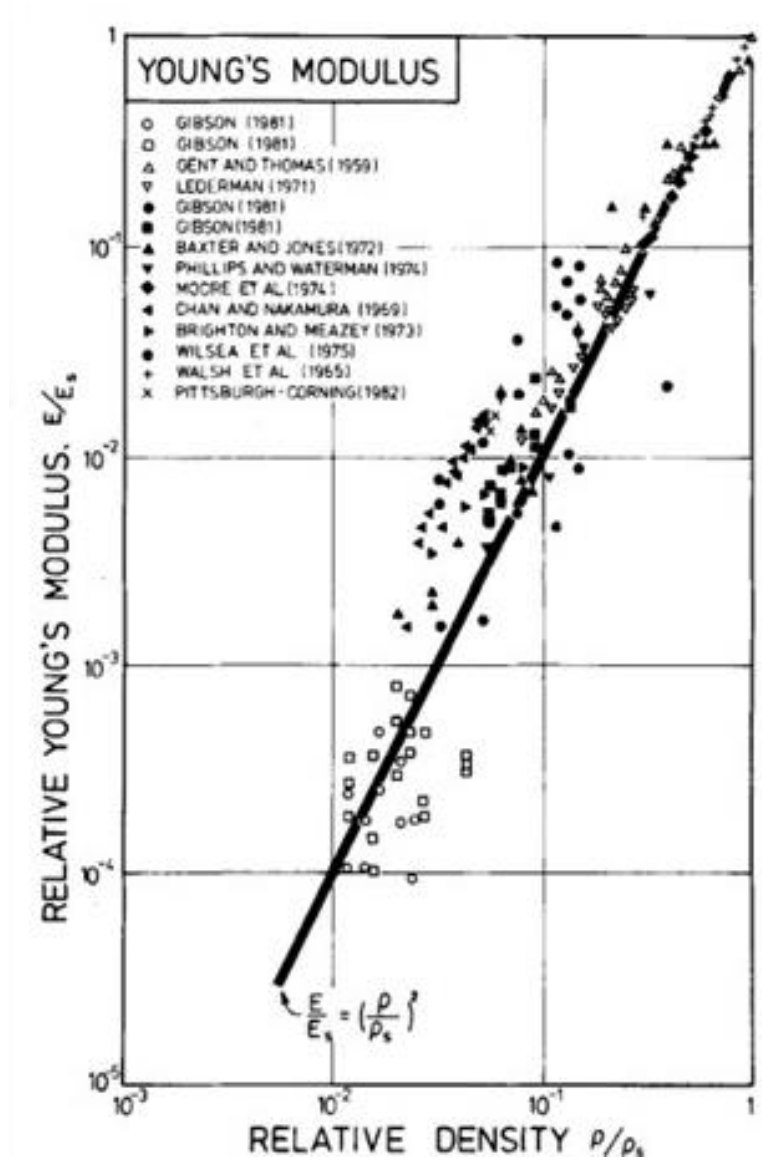


Figure 49. The data used for the Ashby and Mehl model is depicted with the line of fit that was used to develop the relationship between relative modulus and relative density, Equation 6 (38).

log-log domain with relative density on the x-axis and relative modulus or relative compressive strength on the y-axis. Then the data was fit for a relationship. Looking at the data that Ashby and Mehl used for their analysis of both elastic modulus and compressive strength, shown in Figure 49 and Figure 50, there are some apparent

incongruities in the data leading to errors in their models. There is a lot of data that was used to develop the relationship of elastic modulus and relative density, but as the relative density drops below 0.1 and approaches 0.01 the data begins to spread apart and a linear fit is not as clear as it is seen in higher relative densities. This is the same region where the majority of the foam samples used for compression testing fell. The data used to develop the model for elastic modulus is not precise when the relative density approaches 0.01. For the compressive strength data, the amount of data used to develop the model for compressive strength is very limited and spans a limited relative density range. In addition the fit of the data does not appear to work well. There is two distinct regions in the data and Ashby and Mehl fit the data with one equation as opposed to a split function that would apply to two distinct domains. These discrepancies with the Ashby and Mehl model help understand why the data collected does not fit the models already in the literature. Moving forward with the development of ceramic foams improvements on the Ashby and Mehl model needs to be made to link the experimental data to the theoretical models.

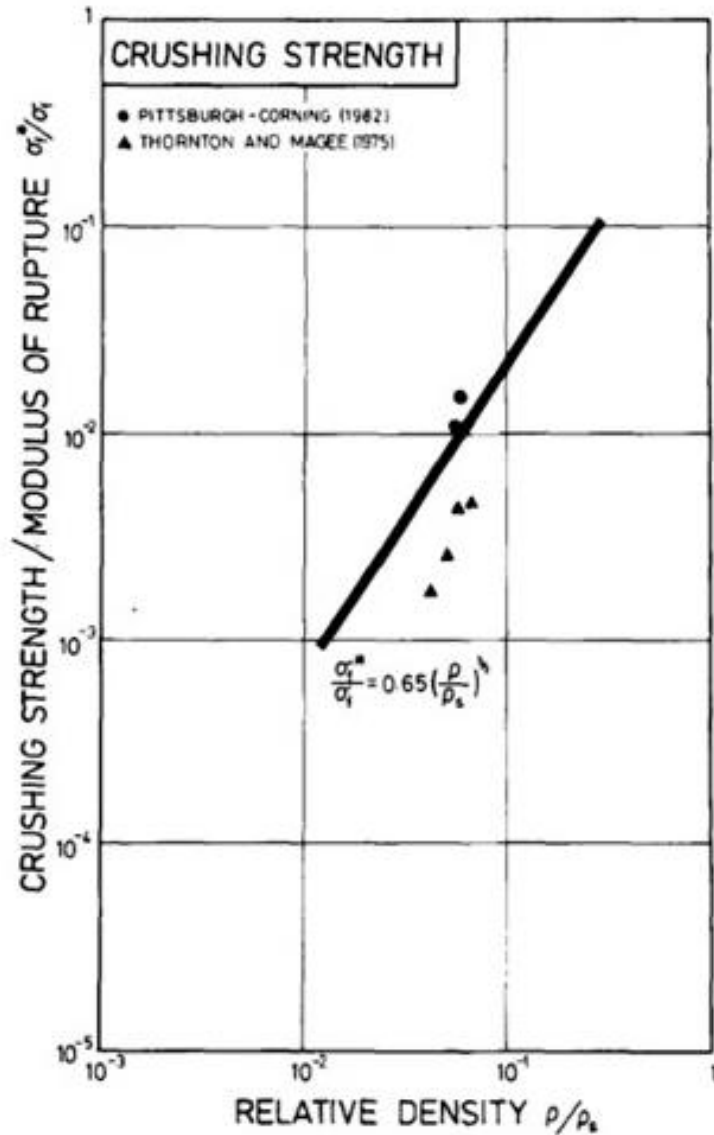


Figure 50. The data used for the Ashby and Mehl model is depicted with the line of fit that was used to develop the relationship between relative compressive strength and relative density, Equation 8 (38).

Sintering Characteristics

Through observations using light microscopy the ability of the foam to sinter into a microporous structure was explored. The majority of green state foams were able to sinter in the struts while being able to maintain the macroporous structure. The only

foams that were not able to sinter properly had a solids loading of 5% with high binder concentration of 2.0 and 3.0. The HA-12 decomposed during the pyrolysis process and the ceramic particles were too spread apart and the structures collapsed from their own weight. Similarly, with the foam sample with a high foam volume expansion ratio the structure collapsed after pyrolysis. Again, once the HA-12 were removed from the structure the ceramic particles were not sintered enough and the structure collapsed from its own weight. The majority of green state foam were able to sinter properly.

Looking at the microstructure of various types of foam it was determined that increased solids loading resulted in higher densification of the grains. In Figure 42 this can be seen as a more uniform, flatter surface. As the solids loading decreases it is seen that the grains of aluminum oxide are easier to spot and less necking has occurred between particles. Interestingly, in the foam type 30/0.7 – 10 pores can be seen running through the struts suggesting that as the foam froze ice crystals excluded the ceramic particles and formed columns in the struts of the foam. These “large” gaps would be impossible for the aluminum oxide particles to jump across, making it impossible for full densification to be possible.

From the microstructure images, Figure 51, the foams that sintered the best were the ones with higher solids loading. This makes sense from a sintering perspective, because the particles would be closer together and diffusion between adjacent particles would take less time to achieve and less energy input to overcome the activation energy.

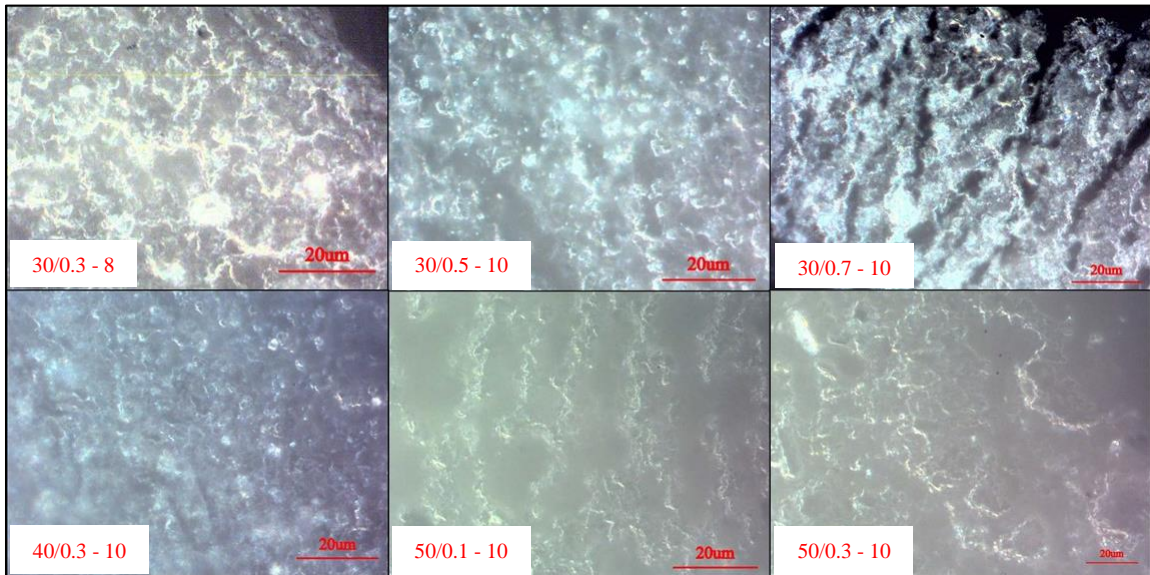


Figure 51. The microstructure of various types of foam shows how well each type of foam densified. The higher solids loading foam samples have more necking and better sintering in the microstructure. Foam type 30/0.7 – 10 has columns within the struts of the foam where ice exclusion has made it impossible for struts to fully densify.

Demonstration of Freeze Foaming with other Material Systems

The majority of the research was performed using aluminum oxide as a model ceramic, but to show that this manufacturing process is applicable to other material systems the freeze foaming process was utilized to synthesize yttria stabilized zirconia (YSZ) foam, copper foam, and aluminum foam.

Yttria Stabilized Zirconia

There were no necessary changes necessary to create Yttria Stabilized Zirconia (YSZ) foam. The powder used to create the foam was 8mol% Yttria Stabilized Zirconia (Tosoh, Kaisei-Cho, Japan). The same dispersant Darvan C-N was utilized at 1.5 wt% (of YSZ) and Rhoplex HA-12 binder was added to ensure proper foaming and stabilization

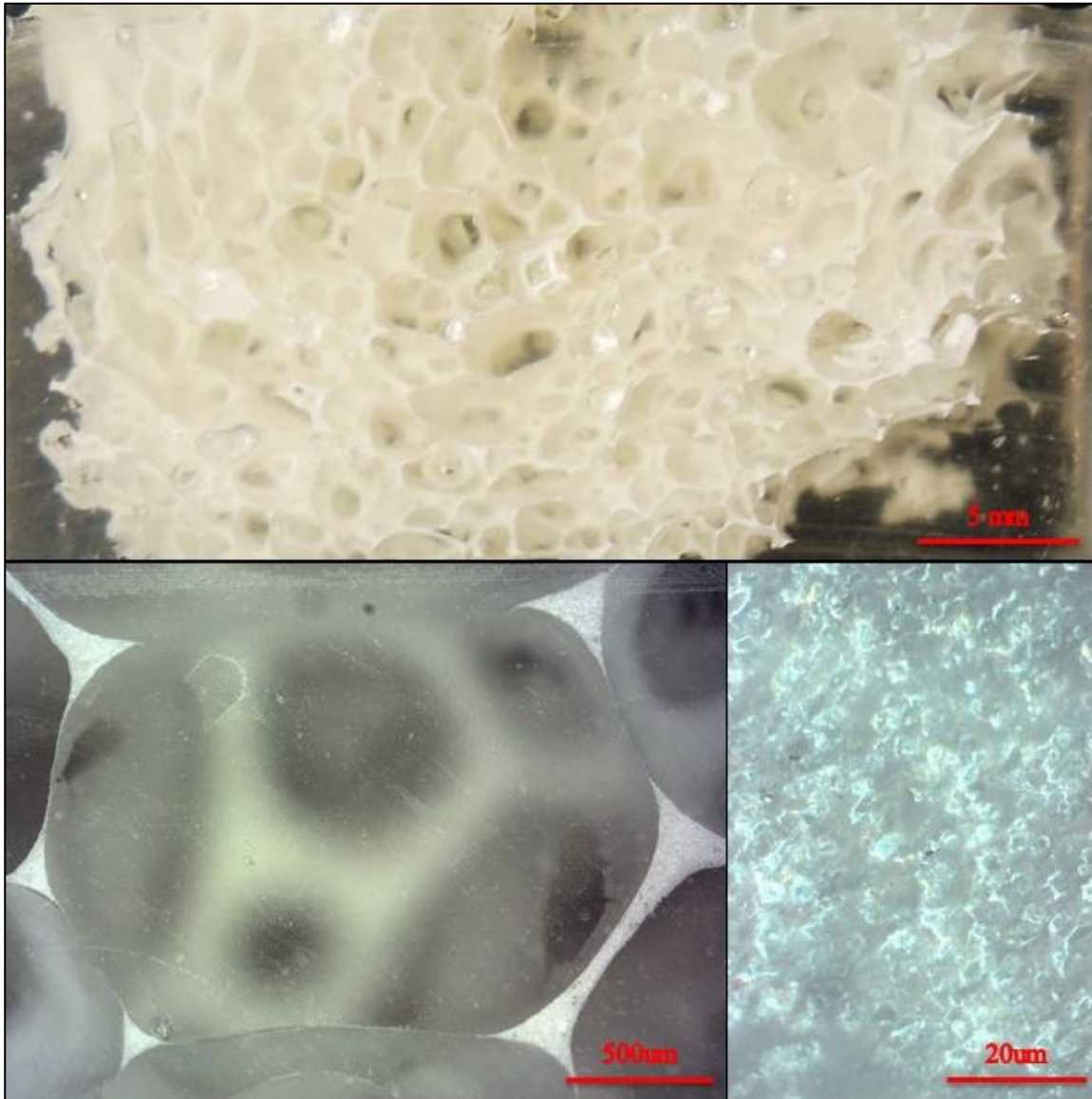


Figure 52. Successfully synthesized YSZ foam done by freeze foaming.

during the freezing process. Figure 52, shows the microstructure, macrostructure, and full cross section of a sample of YSZ foam made using freeze foaming. It can be seen that the foam has a very similar structure to the aluminum oxide foam. It is shown that freeze foaming was able to make an open cell foam with large macroscopic pores and thin struts. In addition, the foam was fully densified through a normal sintering profile like the

one used for the aluminum oxide foam, but it only went to a temperature of 1400°C. There was one additional ingredient used for the YSZ foam. Xanthan gum, a natural thickener, was added to the slurry. The YSZ foam had a solids volume ratio of 25%, a binder concentration of 0.2, and 0.75wt% (of water) xanthan gum.

Metals

To demonstrate that freeze foaming is a robust process it was shown that the process could be used to synthesis metallic foam as well as ceramic foam. Two different types of metals were chosen; aluminum and copper.

To synthesize aluminum foam only one change was necessary. The dispersant used was changed from Darvan-CN to Surfynol CT-234 (Air Products and Chemical, Allentown, PA). The aluminum foam sample can be seen in Figure 43. To synthesize the aluminum foam, 325 mesh aluminum powder (Alfa Aesar, Ward Hill, Ma) was mixed into an aqueous solution at a solids loading of 30% and a binder concentration of 0.3 was utilized. It can be seen that the aluminum foam has the large pores that has been observed with alumina samples, Figure 53. It should be noted that for the sintering process, that the aluminum sample was sintered in air. This caused some oxidation at the surface.

In the case of synthesizing copper foam three changes to the formula were done; the dispersant was changed to Surfynol CT-324, a small amount of Xanthan gum was added, and the binder was changed to Q-PAC 40. Q-PAC 40 (Empower Materials, New Castle, DE) is a binder that is used in ceramic, metallic, and glass material systems that contains polypropylene carbonate. It come in multiple forms, but the form used was an



Figure 53. Aluminum foam made using the freeze foaming process.

aqueous emulsion. Copper foam was synthesized by using a 20% solids loading of 325 mesh copper powder (Alfa Aesar, Ward Hill, Pa), a xanthan gum at 1wt% (of water), and 0.5 binder concentration. During the sintering process, the copper foam was being sintered in a reducing environment but air contamination occurred causing the sample to oxidize. Interestingly enough the copper sample became covered in multiple oxidation states instead of just one. The copper foam did form a similar structure to that seen in the aluminum oxide foam, which can be seen in Figure 54.



Figure 54. Copper foam synthesized using the freeze foaming process. Different oxidation states, indicated by different colors.

CONCLUSIONS

The results of density measurements, compression testing, and light microscopy show the potential of freeze foaming for the manufacturing of high porosity open cell foams from 59 – 94% porosity. The results suggest freeze foaming to be a materials flexible process that can be used to further develop the process for manufacturing non-oxide ceramic and metallic foams.

It was shown that without increasing the viscosity, with additives, of the aqueous slurry that foams could be made with a range of solids loading from 30% to 50%. Also, with an increase in binder concentration the solids loading can be dropped down to 20%. Foam structures were obtained as low as 5% solids loading, but upon sintering the structures collapsed. It was determined that the slurry can be expanded to 15 times its original volume while having the ability to be sintered. Through visual observations, the pore size of lower expanded foams is more consistent, but the relative density of the foam decreases with higher expansion ratios until it reaches a plateau at an expansion ratio of 10. It was also observed that both the elastic modulus and compressive strength increased as a function of relative density.

Due to better sintering properties and mechanical properties while still having a high degree of porosity ceramic slurries comprising of high solids loading and low binder concentrations should be utilized moving forward in the development of freeze foaming. The 50% solids loading foams only saw a decrease in porosity by 4% compared to the 30% solids loading foams, but had significantly high compressive strengths almost a factor of 8 higher compared to foams with a solids loading of 40%. Additionally, the

elastic modulus increased by a factor of 2. The higher mechanical properties were a result of better sintering of the alumina particles within the struts of the foam.

The freeze foaming process has the potential to impact the synthesis of ceramic and metallic foams. Due to the near-net shaped, environmentally friendly, and inexpensiveness of freeze foaming, this process could revolutionize ceramic and metallic foams and see them being used in applications where they were unfeasible previously.

Future Work

For the continued development of freeze foaming there are two different studies that would be beneficial to get more fundamental knowledge about the freeze foaming process. This additional knowledge could help make freeze foaming be a wide spread manufacturing technique for open cell ceramic and metallic foams. First, a rheology study would be useful. Studying the effects of viscosity would help answer some fundamental questions. It would help illustrate the effects of drainage during the foaming process. A rheology study would help with understanding the fundamentals of bubble formation in freeze foaming. In addition, how the ice is forming in the foam. Second, how pressure influences the freeze foaming process would be beneficial. This study would also be able to show insights into the fundamentals of bubble formation in freeze foaming as well as drainage within the foam. A study into the effects of pressure would also be able to help get freeze foaming being used in industry as this would need to be used in machinery to ensure high quality and consistency in the manufacturing process.

REFERENCES CITED

- (1) Huggins, Robert A. "Principles of Ceramics Processing, 2nd Edition: By James S. Reed. John Wiley & Sons, Inc., New York, 1995, Pp. 658, Price \$ 69.95." *Materials Research Bulletin* 30.9 (1995): 1179-182. Web.
- (2) "Montana Museum of Art & Culture." *Montana Museum of Art & Culture - University Of Montana*, www.umt.edu/montanamuseum/exeventsschedule/pastexhibitions/2005-2006.php.
- (3) "Zirconium Implants - Dr. Alison Kerns." *Sophia Health Institute*, 26 Feb. 2017, www.sophiahi.com/zirconium-implants/.
- (4) Loff, Sarah. "April 29, 1990, Discovery Lands Following Hubble Deployment Mission." *NASA*, NASA, 29 Apr. 2015, www.nasa.gov/image-feature/april-29-1990-shuttle-discovery-lands-following-hubble-deployment-mission.
- (5) *Orient-Electrical insulators*, www.suspensioninsulator.com/technic/Electrical-insulators.html.
- (6) Mistler, Richard E., and Eric R. Twiname. *Tape Casting: Theory and Practice*. Westerville, OH: American Ceramic Society, 2000. Print.
- (7) Ashby, Michael, et al. *Materials Engineering, Science, Processing and Design*. 3rd ed., Elsevier, 2014.
- (8) *Material Science and Engineering an Introduction 8th Edition*, Callister/Rethwisch
- (9) Sofie, Stephen. *MTSI 501: Advanced Materials Science I*. Fall 2017, Bozeman, MT, Montana State University.
- (10) Ashby Michael F, and Jones David R.H. *Ceramics*. In *Engineering Materials 2 - An Introduction to Microstructures and Processing*, 2. 4th ed. Elsevier, 2013
- (11) Kotz, John, et al. *Chemistry & Chemical Reactivity*. 8th ed., Brooks/Cole, Cengage Learning, 2012.
- (12) Mehr, Mehrad, et al. "Epoxy interface method enables enhanced compressive testing of highly porous and brittle materials." *Ceramics International*, vol. 42, no. 1, 2016, pp. 1150–1159. doi:10.1016/j.ceramint.2015.09.045.
- (13) Kim, Lee, Han, and Park. "Control of Pore Size in Ceramic Foams: Influence of Surfactant Concentration." *Materials Chemistry and Physics* 113.1 (2009): 441-44. Web.
- (14) Nishihara, Mukai, Yamashita, and Tamon. "Ordered Macroporous Silica by Ice Templating." *Chemistry of Materials* 17.3 (2005): 683-89. Web.

- (15) Gonzenbach, Urs T., André R. Studart, Elena Tervoort, and Ludwig J. Gauckler. "Macroporous Ceramics from Particle-Stabilized Wet Foams." *Journal of the American Ceramic Society* 90.1 (2007): 16-22. Web.
- (16) Luyten, Mullens, Cooymans, De Wilde, Thijs, and Kemps. "Different Methods to Synthesize Ceramic Foams." *Journal of the European Ceramic Society* 29.5 (2009): 829-32. Web..
- (17) Ahmad, Ha, and Song. "Particle-stabilized Ultra-low Density Zirconia Toughened Alumina Foams." *Journal of the European Ceramic Society* 33.13-14 (2013): 2559-564. Web.
- (18) Bienvenu, Yves. "Application and Future of Solid Foams." *Comptes Rendus - Physique* 15.8-9 (2014): 719-30. Web.
- (19) Saye, Robert I, and James A Sethian. "Multiscale Modeling of Membrane Rearrangement, Drainage, and Rupture in Evolving Foams." *Science (New York, N.Y.)* 340.6133 (2013): 720-4. Web.
- (20) C28.04 Advanced Ceramics. "Standard Test Method for Flexural Strength of Advanced Ceramics with Engineered Porosity (Honeycomb Cellular Channels) at Ambient Temperatures." (2011). Web.
- (21) Liu, Xiaoxing, Christophe L. Martin, Didier Bouvard, Stéphane Di Iorio, Jérôme Laurencin, and Gérard Delette. "Strength of Highly Porous Ceramic Electrodes." *Journal of the American Ceramic Society* 94.10 (2011): 3500-508. Web.
- (22) Wucherer, Laurel, Juan C. Nino, Francesco Basoli, and Enrico Traversa. "Synthesis and Characterization of BaTiO₃-Based Foams with a Controlled Microstructure." *International Journal of Applied Ceramic Technology* 6.6 (2009): 651-60. Web.
- (23) Salvo, Martin, Suard, Marmottant, Dendievel, and Blandin. "Processing and Structures of Solids Foams." *Comptes Rendus - Physique* 15.8-9 (2014): 662-73. Web.
- (24) Studart, André R., Urs T. Gonzenbach, Elena Tervoort, and Ludwig J. Gauckler. "Processing Routes to Macroporous Ceramics: A Review." *Journal of the American Ceramic Society* 89.6 (2006): 1771-789. Web.
- (25) Hing, Karin A. "Bioceramic Bone Graft Substitutes: Influence of Porosity and Chemistry." *International Journal of Applied Ceramic Technology* 2.3 (2005): 184-99. Web.

- (26) Sepulveda, Pilar, F. S. Ortega, Murilo D. M. Innocentini, and Victor C. Pandolfelli. "Properties of Highly Porous Hydroxyapatite Obtained by the Gelcasting of Foams." *Journal of the American Ceramic Society* 83.12 (2000): 3021-024. Web.
- (27) G. T. Chandrappa, Nathalie Steunou, and Jacques Livage. "Materials Chemistry: Macroporous Crystalline Vanadium Oxide Foam." *Nature* 416.6882 (2002): 702-702. Web.
- (28) Bin LI, Yong Ya Wang, and Wen Qin Luo. "Preparation and Characterization of Fe₂O₃-CaO-SiO₂ Porous Glass Ceramics for Bacteria Immobilization." *Medžiagotyra* 23.4 (2017): 356-61. Web.
- (29) Seuba, Jordi, Sylvain Deville, Christian Guizard, and Adam J Stevenson. "Mechanical Properties and Failure Behavior of Unidirectional Porous Ceramics." *Scientific Reports* 6.1 (2016): 24326. Web.
- (30) Young, F. Ronald., and Project Muse. *Fizzics: The Science of Bubbles, Droplets, and Foams*. Baltimore, Md.: Johns Hopkins UP, 2011. Book Collections on Project MUSE. Web.
- (31) Chen, Jing-Yin, and Yoo, Choong-Shik. "High Density Amorphous Ice at Room Temperature." *Proceedings of the National Academy of Sciences of the United States* 108.19 (2011): 7685-7688. Web.
- (32) Hunt, Clay. "Sintering in Ceramics and Solid Oxide Fuel Cells." *Montana State University*, 2017. Print.
- (33) Szafran, Mikolaj, Agnieszka Szudarska, and Paulina Bednarek. "New Low Toxic Water-Soluble Monomers for Gelcasting of Ceramic Powders." *Advances in Science and Technology* 62 (2010): 163-68. Web.
- (34) Lyckfeldt, and Ferreira. "Processing of Porous Ceramics by 'starch Consolidation'." *Journal of the European Ceramic Society* 18.2 (1998): 131-40. Web.
- (35) Gonzenbach, Urs T., Andre R. Studart, Elena Tervoort, and Ludwig J. Gauckler. "Ultrastable Particle-Stabilized Foams." *Angewandte Chemie International Edition* 45.21 (2006): 3526-530. Web.
- (36) Han, Chang Dae. *Polymer Processing* (2007). Web.
- (37) "Pilot Scale 2.5"-3.5" Tandem Extrusion System." *Pilot Scale Tandem Extrusion*. N.p., n.d. Web.
- (38) Ashby, M. F., and R. F. Mehl Medalist. "The Mechanical Properties of Cellular Solids." *Metallurgical Transactions A* 14.9 (1983): 1755-769. Web.

- (39) *Darvan C-N*; MSDS No. 13710; Vanderbilt Minerals, LLC: Norwalk, CT.
https://www.vanderbiltminerals.com/publicDocuments/SDS/13710_DARVAN-CN_US_EN_VC-VM.pdf.
- (40) *Rhoplex HA-12*; Rohm and Haas: Spring House, PA.
https://www.dow.com/assets/attachments/business/pbm/rhoplex_ha/rhoplex_ha_12/tds/rhoplex_ha-12.pdf.
- (41) Schumann, M., and L. San-Miguel. "Fiber-Free Ceramic Insulation Foam for Highest Temperatures - a New Generation of HSE-friendly Refractory Products with Multiple Application Possibilities." *Refractories WORLDFORUM* (2017): 1-6. Web.
- (42) Zhu, W. C., and C. A. Tang. "Micromechanical Model for Simulating the Fracture Process of Rock." *Rock Mechanics and Rock Engineering* 37.1 (2004): 25-56. Web.
- (43) Jayasinghe, S.N., and M.J. Edirisinghe. "A Novel Method of Forming Open Cell Ceramic Foam." *Journal of Porous Materials* 9.4 (2002): 265-73. Web.
- (44) Hong, Changqing, Zhang, Xinghong, Han, Jiecai, Du, Jiancong, and Han, Wenbo. "Ultra-high-porosity Zirconia Ceramics Fabricated by Novel Room-temperature Freeze-casting." *Scripta Materialia* 60.7 (2009): 563-66. Web.
- (45) Li, Peixu, Zhen Li, Luhui Zhang, Enzheng Shi, Yuanyuan Shang, Anyuan Cao, Hongbian Li, Yi Jia, Jinquan Wei, Kunlin Wang, Hongwei Zhu, and Dehai Wu. "Bubble-promoted Assembly of Hierarchical, Porous Ag₂S Nanoparticle Membranes." *Journal of Materials Chemistry* 22.47 (2012): 24721. Web.